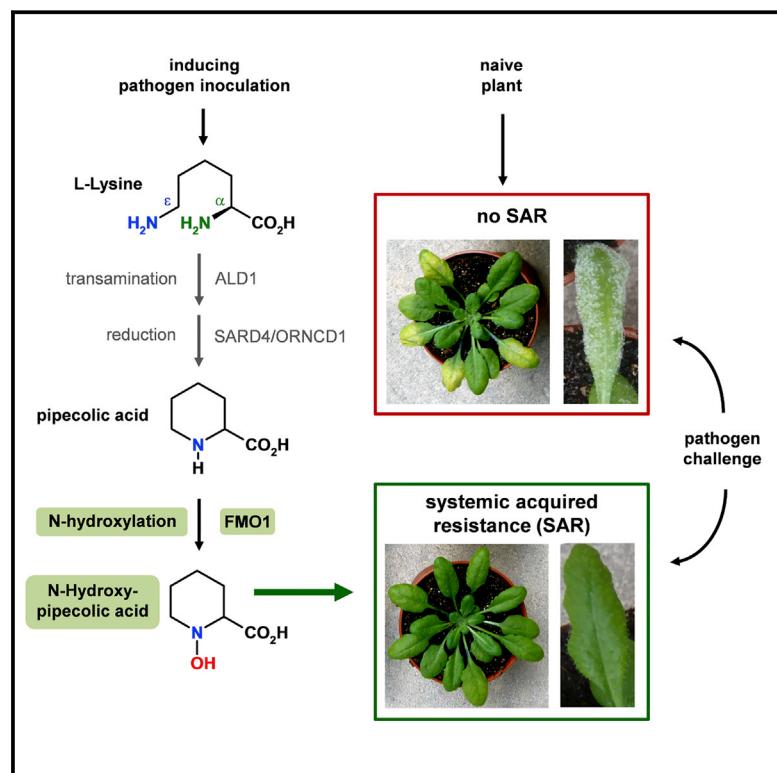


Flavin Monooxygenase-Generated N-Hydroxypipelicolic Acid Is a Critical Element of Plant Systemic Immunity

Graphical Abstract



Authors

Michael Hartmann, Tatyana Zeier, Friederike Bernsdorff, ..., Torsten Hölzel, Christian Ganter, Jürgen Zeier

Correspondence

juergen.zeier@hhu.de

In Brief

A pathogen-inducible L-Lys catabolic pathway in plants generates N-hydroxypipelicolic acid as a critical regulator of systemic acquired resistance to pathogen infection.

Highlights

- Pipecolic acid (Pip) induces systemic acquired resistance dependent on FMO1
- FMO1 catalyzes the hydroxylation of Pip to N-hydroxypipelicolic acid (NHP)
- NHP accumulates systemically in the plant foliage in response to pathogen attack
- NHP induces systemic acquired resistance to bacterial and oomycete infection



Flavin Monooxygenase-Generated N-Hydroxypipicolinic Acid Is a Critical Element of Plant Systemic Immunity

Michael Hartmann,¹ Tatyana Zeier,¹ Friederike Bernsdorff,¹ Vanessa Reichel-Deland,¹ Denis Kim,¹ Michele Hohmann,¹ Nicola Scholten,¹ Stefan Schuck,^{1,2} Andrea Bräutigam,^{2,3,5} Torsten Hölzel,⁴ Christian Ganter,⁴ and Jürgen Zeier^{1,2,6,*}

¹Institute for Molecular Ecophysiology of Plants, Department of Biology, Heinrich Heine University, Universitätsstraße 1, 40225 Düsseldorf, Germany

²Cluster of Excellence on Plant Sciences (CEPLAS), Heinrich Heine University, Universitätsstraße 1, 40225 Düsseldorf, Germany

³Institute for Plant Biochemistry, Department of Biology, Heinrich Heine University, Universitätsstraße 1, 40225 Düsseldorf, Germany

⁴Institute of Inorganic and Structural Chemistry, Department of Chemistry, Heinrich Heine University, Universitätsstraße 1, 40225 Düsseldorf, Germany

⁵Present address: Faculty of Biology, Computational Biology, University of Bielefeld, Universitätsstraße 27, 33615 Bielefeld, Germany

⁶Lead Contact

*Correspondence: juergen.zeier@hhu.de

<https://doi.org/10.1016/j.cell.2018.02.049>

SUMMARY

Following a previous microbial inoculation, plants can induce broad-spectrum immunity to pathogen infection, a phenomenon known as systemic acquired resistance (SAR). SAR establishment in *Arabidopsis thaliana* is regulated by the Lys catabolite pipicolinic acid (Pip) and flavin-dependent-monoxygenase1 (FMO1). Here, we show that elevated Pip is sufficient to induce an FMO1-dependent transcriptional reprogramming of leaves that is reminiscent of SAR. *In planta* and *in vitro* analyses demonstrate that FMO1 functions as a pipecolate N-hydroxylase, catalyzing the biochemical conversion of Pip to N-hydroxypipicolinic acid (NHP). NHP systemically accumulates in plants after microbial attack. When exogenously applied, it overrides the defect of NHP-deficient *fmo1* in acquired resistance and acts as a potent inducer of plant immunity to bacterial and oomycete infection. Our work has identified a pathogen-inducible L-Lys catabolic pathway in plants that generates the N-hydroxylated amino acid NHP as a critical regulator of systemic acquired resistance to pathogen infection.

INTRODUCTION

Flavin-containing monooxygenases (FMOs) are widely conserved enzymes in prokaryotes, fungi, animals, and plants. FMOs contain a flavin adenine dinucleotide (FAD) prosthetic group and commonly monooxygenate the S- or N-atoms of small nucleophilic substrates by the transfer of one O-atom from molecular oxygen and the consumption of reducing equivalents from NAD(P)H (Rossner et al., 2017). The genome of the model plant *Arabidopsis thaliana* (*Arabidopsis*) contains 29 genes coding for proteins with significant sequence similarity to human

FMOs. Plant FMO genes have been divided into three clades (Schlauch, 2007). Clade II contains the 11 *Arabidopsis YUCCA* genes involved in the biosynthesis of the plant hormone indole-3-acetic acid (Mashiguchi et al., 2011), and the clade III FMOs characterized thus far are involved in the S-oxygenation of sulfides to sulfoxides within the biosynthesis of sulfur-containing plant secondary metabolites (Li et al., 2008; Yoshimoto et al., 2015).

The clade I of plant FMOs contains only two *Arabidopsis* genes, the highly pathogen-inducible gene *flavin-dependent-monoxygenase1* (*FMO1*) and a pseudogene (Schlauch, 2007). In 2006, three independent studies provided complementary evidence that *FMO1* holds an important function in *Arabidopsis* immunity to microbial pathogen invasion (Bartsch et al., 2006; Koch et al., 2006; Mishina and Zeier, 2006). Intact *FMO1* is required for proper basal immunity of *Arabidopsis* to virulent isolates of the oomycete *Hyaloperonospora arabidopsidis* (*Hpa*), the causal agent of downy mildew, and to compatible strains of the bacterial pathogen *Pseudomonas syringae*. In addition, *fmo1* knockout mutants exhibit compromised specific immunity to adapted pathogens triggered by the TIR-NB-LRR subclass of plant resistance (R) genes (Bartsch et al., 2006; Koch et al., 2006).

Functional *FMO1* is indispensable for the induction of systemic acquired resistance (SAR) (Mishina and Zeier, 2006), an inducible immune response of plants that is triggered by a localized microbial inoculation and provides broad-spectrum resistance in the entire foliage to future attack (Shah and Zeier, 2013; Fu and Dong, 2013). SAR establishment is controlled by the immune-regulatory metabolites salicylic acid (SA) and pipecolic acid (Pip) (Nawrath and Métraux, 1999; Návárová et al., 2012). Upon SAR induction, both metabolites accumulate in the inoculated (1°) leaves and in the non-inoculated, systemic (2°) leaves (Bernsdorff et al., 2016). The stress-related biosynthesis of SA in *Arabidopsis* is derived from chorismate and requires the pathogen-inducible *isochorismate synthase1* (*ICS1*) gene (Wildermuth et al., 2001). Accumulating SA activates the transcriptional co-regulator non-expressor of PR genes1 (NPR1) to induce plant pathogen resistance (Fu and Dong, 2013).



In *Arabidopsis*, Pip is synthesized by a two-step biochemical process from L-Lys (Ding et al., 2016; Hartmann et al., 2017). The aminotransferase AGD2-like defense response protein1 (ALD1) abstracts the α -amino group from L-Lys to form 2,3-dehydropipecolic acid (2,3-DP). 2,3-DP is subsequently reduced to Pip by action of SAR-deficient4 (SARD4) and an additional reductive activity (Hartmann et al., 2017). Similar to *FMO1*, both *ALD1* and *SARD4* are systemically upregulated in the foliage of pathogen-inoculated plants (Song et al., 2004; Mishina and Zeier, 2006; Hartmann et al., 2017). The resulting accumulation of Pip in leaves is necessary for SAR induction and the establishment of a conditioned state that primes plants for enhanced defense activation during subsequent attack (Návarová et al., 2012). Pip triggers SAR and defense priming by a major, SA-dependent and a minor, SA-independent signaling mode (Bernsdorff et al., 2016). Notably, the induction of acquired resistance and priming by Pip requires functional *FMO1*, indicating that the *FMO1* monooxygenase is a critical downstream component in the Pip resistance pathway (Návarová et al., 2012).

In the present study, we identify the biochemical function of *FMO1* as pipecolate N-hydroxylase, catalyzing the biosynthesis of the as yet undescribed N-hydroxylated amino acid N-hydroxypipecolic acid (NHP) from Pip. Upon pathogen inoculation, NHP accumulates systemically in the *Arabidopsis* foliage and induces SAR to *P. syringae* and *Hpa* infection. Our work has thus identified a pathogen-inducible L-Lys catabolic pathway with a central function in plant immunity.

RESULTS

Transcriptional Reprogramming by Pip is *FMO1*-Dependent and Constitutes an Integral Part of SAR

A SAR-inducing inoculation of a 1° leaf with *P. syringae* pv. *maculicola* (*Psm*) triggers a strong transcriptional response in distant 2° leaves in dependence of endogenously accumulating Pip and functional *FMO1* (Gruner et al., 2013; Bernsdorff et al., 2016). To investigate whether elevations of Pip are sufficient for a SAR-like transcriptional reprogramming, we supplied individual *Arabidopsis* Col-0 plants with doses of 10 μ mol Pip and determined the response in leaves 1 day later by RNA sequencing (RNA-seq) analyses. We directly compared the transcriptional response to Pip with the transcriptional SAR response, i.e., the response of 2° leaves toward a localized *P. syringae* inoculation of 1° leaves (Figure 1) (Bernsdorff et al., 2016).

In the leaves of Pip-supplemented Col-0 plants, 705 genes were found significantly upregulated (Pip⁺ genes) compared to leaves of water-treated control plants (Figure 1A; Table S1). Comparatively, biological SAR induction by *Psm*-inoculation resulted in the systemic upregulation of ~3,200 genes (SAR⁺ genes) (Figure 1B; Table S2) (Bernsdorff et al., 2016). 98% of the Pip⁺ genes (692 out of 705) represented SAR⁺ genes, indicating that the response to elevated Pip is an integral part of the overall transcriptional SAR⁺-response (Figure 1B). The Pip⁺-fraction of the SAR⁺ genes comprised the most strongly upregulated genes in biological SAR, because the mean-fold transcriptional change (*Psm*/mock) in the distal leaves of *Psm*-inoculated plants was markedly higher for the 692 Pip-

regulated (9.1-fold) compared to the remaining 2,525 SAR⁺ genes (3.5-fold) (Figure 1C). Moreover, the SAR⁺ genes, and in particular the Pip⁺ genes, were significantly enriched in SA- and H₂O₂-regulated but not in jasmonate- or abscisic acid-responsive genes (Figure 1C).

Elevated Pip levels are thus sufficient to activate a core part of the transcriptional SAR⁺ response and SAR-like resistance (Figure 1B) (Návarová et al., 2012; Bernsdorff et al., 2016). Biological SAR is also associated with the downregulation of ~3,000 genes, and this SAR⁻ gene group is strongly enriched in photosynthesis- and growth-related genes (Figure 1B) (Bernsdorff et al., 2016). Exogenous Pip only triggered the downregulation of 89 genes, 92% of which are also SAR⁻ genes (Figure 1B). Therefore, the overall Pip⁻ response was modest compared to the SAR⁻ or the Pip⁺ responses.

We next examined whether the 705 Pip⁺ genes were significantly enriched or depleted in particular MapMan categories and *Arabidopsis* gene families (<http://www.arabidopsis.org/>). Among the main MapMan bins, the categories “biotic stress” and “signaling” showed the greatest enrichment (Figure 1D). Moreover, the terms “abiotic stress,” “redox,” and “transport” were significantly enriched among the Pip⁺ genes, whereas the categories “photosynthesis,” “DNA,” “RNA,” “microRNA,” and “protein” were significantly depleted (Figure 1D). Other main MapMan bins were not affected. Notably, gene families associated with the perception of pathogens (nucleotide binding site [NBS]-containing R proteins, receptor-like protein kinases, receptor-like proteins), involved in defense signaling (e.g., calcium and mitogen-activated protein kinase [MPK] signaling), and stress-related transcription factor families (WRKY, NAC) were strongly enriched within the Pip⁺ genes (Figures S1A–S1C), indicating that Pip activates distinct stages of plant defense signaling. Further, at the levels of MapMan categories, subcategories, and gene families, a high qualitative similarity between the Pip⁺ and SAR⁺ responses was evident (Figures 1D and S1).

The RNA-seq data also revealed that elevated Pip is sufficient to upregulate a whole battery of important plant immune-related and SAR-relevant genes. These include metabolic and regulatory genes of SA biosynthesis, genes involved in SA perception and signal transduction, the key genes of Pip biosynthesis (*ALD1*, *SARD4*) and downstream signaling (*FMO1*), and several main regulators of plant basal and race-specific immunity to biotrophic and hemibiotrophic pathogens (Figure S2A). Pip thus activates main players of plant immunity and SAR at the level of transcription. Importantly, the prominent Pip-inducible transcriptional response observed in the wild-type was absent in the *fmo1* mutant. In *fmo1*, only two genes were weakly upregulated upon Pip-treatment, and not a single gene was downregulated (Figures 1A and S2B). Thus, just like the Pip-triggered resistance and priming reactions (Návarová et al., 2012; Bernsdorff et al., 2016), the entire transcriptional response to Pip requires functional *FMO1*.

Flavin-Dependent Monooxygenase1 Functions as a Pipecolic Acid N-Hydroxylase

We previously hypothesized that *FMO1* might metabolize Pip to an N-oxidized derivative required for immune activation (Zeier, 2013). To elucidate the biochemical function of the *FMO1*

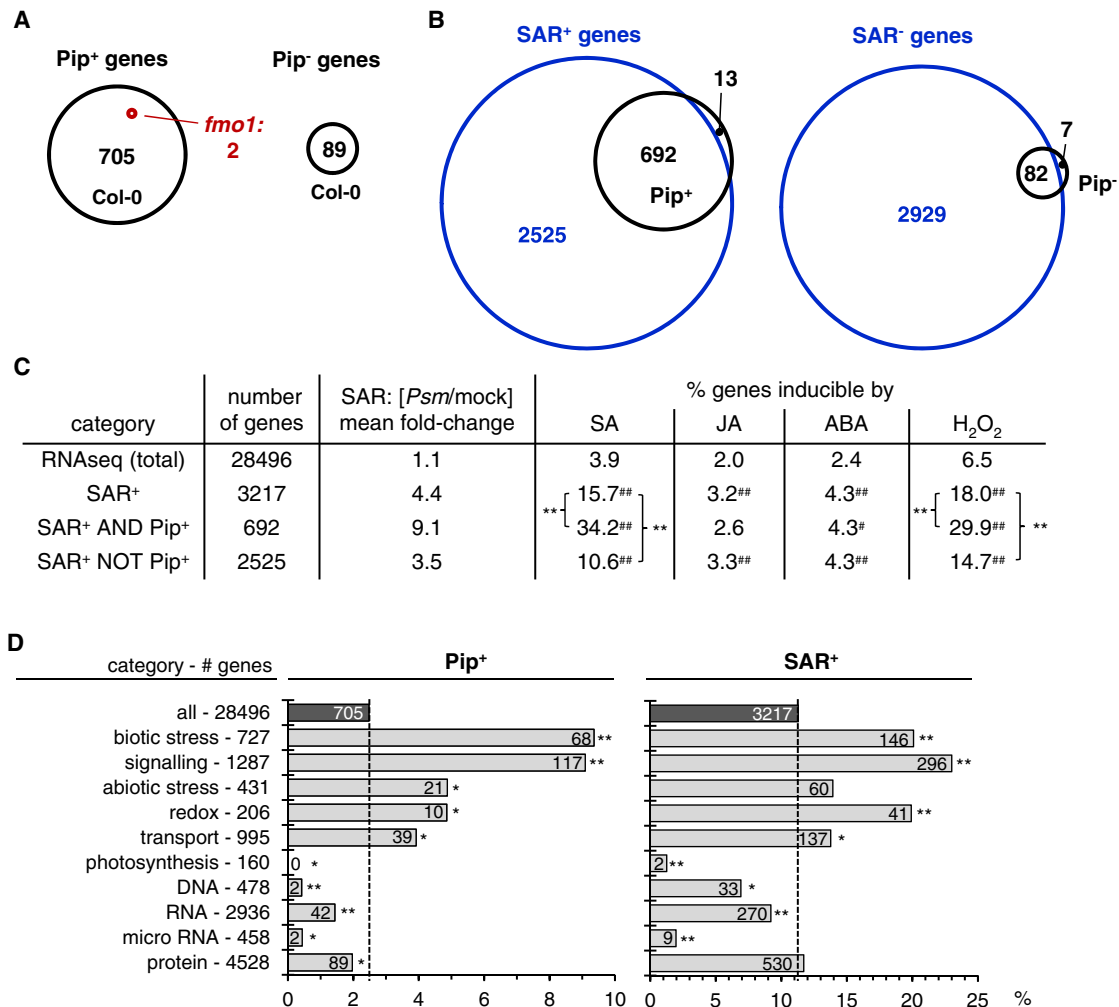


Figure 1. The Transcriptional Response to Elevated Pip Is an Integral Part of SAR Transcriptional Reprogramming and Depends on *FMO1*

(A) Venn diagrams with numbers of differentially regulated genes between Pip⁻ and control-treatments in leaves of *Arabidopsis* Col-0 (black) and *fmo1* (red) (false discovery rate [FDR] <0.05). Left (right): significantly upregulated (downregulated) genes. The Col-0 genes correspond to the Pip⁺ (Pip⁻) genes. One day after treatment of 5-week-old plants with 10 μ Mol Pip or water, gene expression in leaves was analyzed by RNA-seq analysis with 3 biological replicates (n) for each treatment.

(B) Venn diagram illustrating overlap between Pip⁺ and SAR⁺ genes (left) and Pip⁻ and SAR⁻ genes (right). Black: Pip-regulated genes, blue: SAR genes. The SAR⁺ (SAR⁻) genes are upregulated (downregulated) in 2^o leaves of 5-week-old Col-0 plants inoculated 2 days before in 1^o leaves with *Psm*, as compared to a mock-treatment (FDR <0.05; n = 3) (Bernsdorff et al., 2016).

(C) Mean fold-change (*Psm*/mock) in SAR of genes belonging to different categories (column 3), and percentage of genes inducible by salicylic acid (SA), jasmonic acid (JA), abscisic acid (ABA), and H₂O₂ in these categories (columns 4 to 7) (based on sets of 1,105 SA-inducible, 580 JA-inducible, 675 ABA-inducible, and 1,862 H₂O₂-inducible *Arabidopsis* genes) (Gruner et al., 2013). Significant enrichments of the categories in hormone-inducibles genes in relation to the total RNA-seq group are indicated with dashes, and differences between subgroups are indicated by asterisks (**p < 0.001; *p < 0.05; Fisher's exact test).

(D) Proportions of Pip⁺ (left) and SAR⁺ (right) genes in main MapMan functional categories. Dashed vertical lines illustrate the percentage of Pip⁺ and SAR⁺ genes in the whole, RNA-seq-covered transcriptome (28,496 genes). The total number (#) of genes in each category is indicated on the left. The absolute numbers of Pip⁺ and SAR⁺ genes within a particular gene category is indicated on the horizontal bars. Asterisks indicate significant enrichment (or depletion) of gene categories in Pip⁺ or SAR⁺ genes (**p < 0.001; *p < 0.05; Fisher's exact test).

See also Figures S1 and S2 and Tables S1 and S2.

monooxygenase, we performed comparative gas chromatography-mass spectrometry (GC-MS)-based metabolite analyses of leaf extracts from *Psm*-inoculated and control plants of wild-type Col-0, *ald1*, and *fmo1*. We first applied sample derivatization with trimethylsilyl-diazomethane to convert analytes with free carboxylic acid groups into methyl esters which facilitates

their GC-MS analyses (Hartmann et al., 2017). Analyses of GC-MS ion chromatograms of mass-to-charge ratio (m/z) 100 identified a specific substance peak (1a) in the leaf samples of the *Psm*-treated wild-type plants that was absent in any of the mock-control samples, and in samples of *Psm*-treated *ald1* and *fmo1* (Figure 2A). The mass spectrum of 1a exhibited a

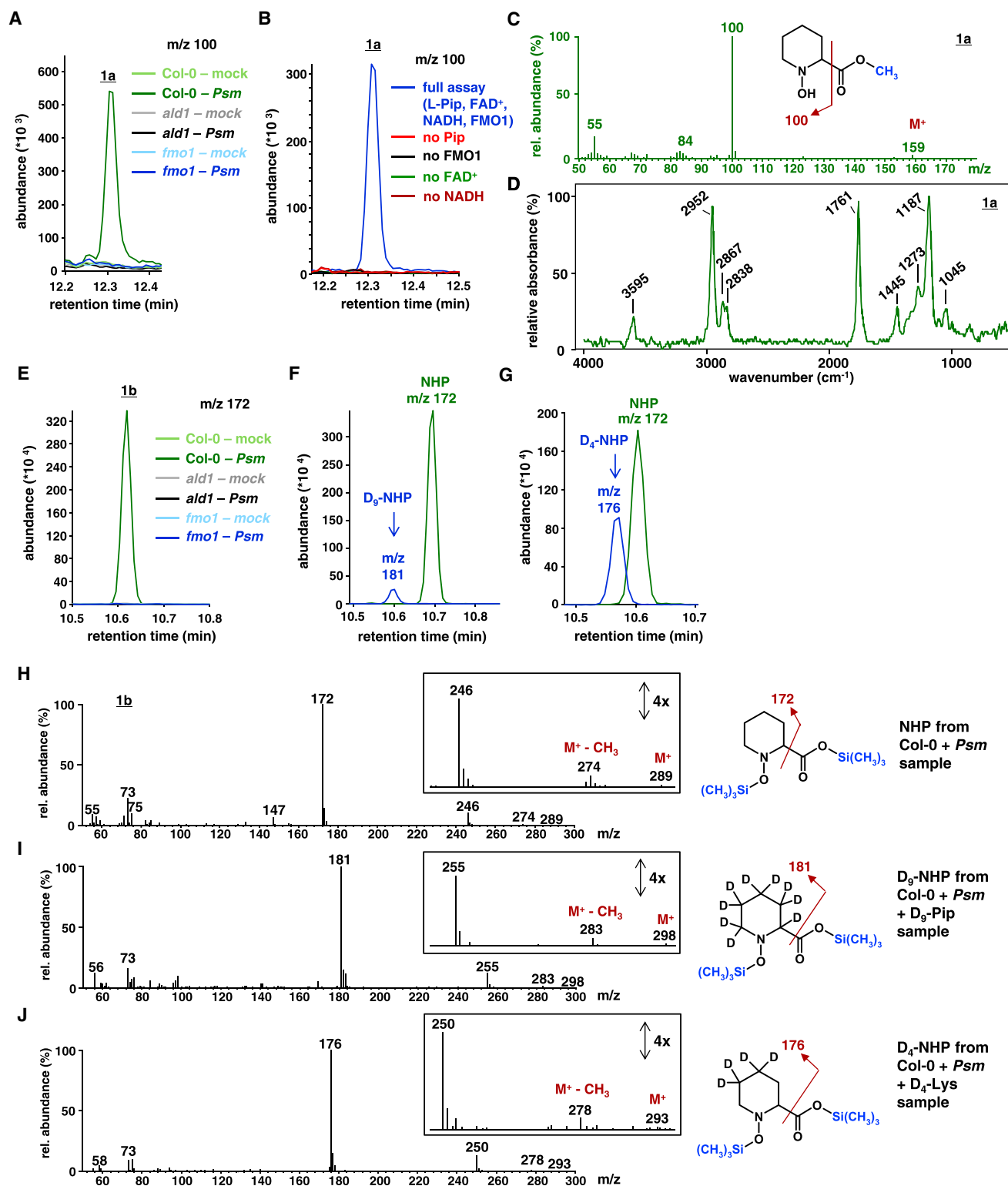


Figure 2. FMO1 Functions as a Pip N-Hydroxylase and Catalyzes N-Hydroxy-Pip Formation *In Vivo* and *In Vitro*

(A) N-hydroxy-Pip (NHP) accumulates in wild-type Col-0 plants but not in *ald1* and *fmo1* after *P. syringae* inoculation. Overlaid ion chromatograms ($m/z = 100$) of GC-MS-analyzed extract samples from mock-treated or *Psm*-inoculated leaves (48 hpi) of Col-0, *ald1*, and *fmo1* plants after sample derivatization by methylation. The molecular species **1a** is exclusively present in the Col-0 - *Psm* samples (green).

(legend continued on next page)

dominant m/z 100 ion (a possible N-hydroxypiperidine fragment) and a putative M^+ ion of m/z 159, which corresponds to the mass of methylated (i.e., derivatized) N-hydroxypipicolinic acid (Figure 2C).

We applied gas chromatography-Fourier transform infrared spectroscopy (GC-FTIR) to obtain an infrared (IR) spectrum of **1a** (Figure 2D). The IR spectrum showed close similarity to a spectrum in the IR database, N-methyl-pipicolinic acid methyl-ester, but possessed an additional band at $3,595\text{ cm}^{-1}$ that is characteristic for O-H stretching vibrations (Figures 2D, S3A, and S3B). This corroborated the assumption that substance **1a** might represent derivatized N-hydroxypipicolinic acid. We chemically synthesized N-hydroxypipicolinic acid (1-hydroxypiperidine-2-carboxylic acid) according to a protocol of Murahashi and Shiota (1987) and characterized the substance by nuclear magnetic resonance (NMR) spectroscopy, mass spectrometry, and elemental analysis (Figure S3G). GC-MS analysis of derivatized samples showed that the mass spectra and retention times of the synthetically generated N-hydroxypipicolinic acid and the identified plant-derived substance were identical (Figures S3C, S3E, and S3F), demonstrating that *Arabidopsis* produces NHP in an *ALD1*- and *FMO1*-dependent manner in response to *Psm* inoculation.

To test the enzymatic activity of FMO1, we overexpressed C-terminally polyhistidine-tagged FMO1 enzyme in *Escherichia coli* and purified the protein via affinity chromatography. L-Pip was tested *in vitro* as a substrate of recombinant FMO1 enzyme in the presence of the presumed co-factors FAD^+ and NADH. After incubation of the assays overnight at 30°C , FMO1 assays were stopped and derivatized with trimethylsilyl-diazomethane to produce methyl esters of substrates and reaction products and analyzed via GC-MS. In the presence of FAD^+ and NADH as cofactors, purified FMO1 protein was able to catalyze the conversion of L-Pip to NHP in the *in vitro* assays, whereas none of the controls, lacking either the substrate, purified FMO1 or one of the co-factors, led to the N-hydroxylation of L-Pip to produce NHP (Figures 2B, S3D, and S3F).

To quantify NHP in plant tissue, we developed a second GC-MS-based method that employs trimethylsilylation of hydroxyl- and amino-groups of the sample analytes. With this procedure, NHP is silylated both at the N-OH and the carboxyl OH group.

The mass spectrum of the derivatized NHP (**1b**) shows a dominant ion of m/z 172, a weak but discernable M^+ ion at m/z 289, and a M^+-CH_3 fragment ion at m/z 274 (Figure 2H). By use of the single ion chromatogram of m/z 172, NHP could be robustly quantified in plant extracts (Figure 3), and comparative extract analyses confirmed that NHP is only biosynthesized in *Psm*-inoculated Col-0 but not in *ald1* or *fmo1* (Figure 2E). To further define the biosynthetic pathway of NHP in *Arabidopsis*, we fed plants with isotope-labeled D_9 -Pip and concomitantly inoculated them with *Psm*. In doing so, we observed the *in planta* generation of D_9 -labeled NHP in addition to the unlabeled compound (Figures 2F and 2I). Similarly, when 4,4,5,5- D_4 -Lys was co-applied with *Psm* to plants, we detected, in addition to D_4 -labeled Pip (Hartmann et al., 2017), the co-occurrence of the corresponding D_4 -labeled NHP in the extracts (Figures 2G and 2J). Isotope-labeled D_9 -NHP (from D_9 -Pip feeding) and D_4 -NHP (from D_4 -Lys feeding) were also detected with the alternative GC-MS procedure that used analyte derivatization by methylation (Figures S4A–S4D). In addition, when feeding the Lys isotopic variant L-Lys-6- ^{13}C , ϵ - ^{15}N to *Psm*-inoculated Col-0, the *in planta* generation of ^{13}C , ^{15}N -labeled NHP was observed (Figure S4E). Together, our *in planta* and *in vitro* studies demonstrate that *Arabidopsis* produces NHP in response to pathogen inoculation by the FMO1-catalyzed N-hydroxylation of L-Pip (Figures 2, S3, and S4), which itself is biosynthesized via an *ALD1*-mediated α -transamination of L-Lys (Hartmann et al., 2017).

N-Hydroxypipicolinic Acid Accumulates Systemically in the *Arabidopsis* Foliage at the Onset of Biological SAR

To characterize the endogenous generation of NHP in *Arabidopsis* in response to pathogen attack, we determined the levels of NHP in 1° and 2° leaves of Col-0 plants at different times after *Psm*-inoculation and mock-treatment. Over the entire time course, NHP was not detected in the mock-control plants (Figure 3A). In *Psm*-inoculated 1° leaves, however, NHP was produced from 10 hr post inoculation (hpi) onward, with the onset of local NHP generation coinciding with the rise of Pip (Figures 3A and S5A). At 24 hpi, the NHP levels reached a maximum of $\sim 30\text{ }\mu\text{g g}^{-1}\text{ FW}$, which was quantitatively similar to the amount of Pip that had accumulated at this stage of infection (Figures 3A and S5A). At 48 hpi, the levels of NHP decreased to about

(B) Biochemical *in vitro* assays with recombinant FMO1, as analyzed by GC-MS after analyte derivatization by methylation. Overlaid ion chromatograms ($m/z = 100$) are shown. Substance **1a** is detected as the reaction product in full enzyme assays containing $50\text{ }\mu\text{g mL}^{-1}$ FMO1, $200\text{ }\mu\text{M}$ FAD^+ , $400\text{ }\mu\text{M}$ NADH, and 10 mM L-Pip as the substrate (blue), but not in control assays lacking either L-Pip (red), FMO1 protein (black), FAD^+ cofactor (green), or NADH (red brown).

(C) Mass spectrum of **1a** from Col-0 extract samples, which is identical to the spectra of the enzymatically generated substance and of chemically synthesized, authentic N-hydroxy-Pip (Figures S3C–S3E). The chemical structure of methylated (derivatized) NHP, the molecular ion (M^+), and the main fragmentation (m/z 100) are indicated. The methyl group (blue) is introduced by sample derivatization.

(D) Infrared (IR) spectrum of **1a**, as determined by GC-FTIR spectroscopic analysis. Assignments of main IR bands to functional group vibrations (wave number/vibration): $3,595\text{ cm}^{-1}$ /O-H stretching; $2,952\text{ cm}^{-1}$ /C-H (methyl) stretching; $2,867$ and $2,838\text{ cm}^{-1}$ /C-H (methylene) stretching; $1,761\text{ cm}^{-1}$ /C=O stretching; $1,187\text{ cm}^{-1}$ /C-O stretching.

(E) Overlaid ion chromatograms ($m/z = 172$) of GC-MS-analyzed extract samples from mock-treated or *Psm*-inoculated leaves (48 hpi) of Col-0, *ald1*, and *fmo1* plants after sample derivatization by trimethylsilylation. Bis-trimethylsilylated NHP **1b** is exclusively detected in the Col-0-*Psm* samples (dark green).

(F and G) NHP is biosynthetically derived from Pip and L-Lys in plants. Feeding of isotope-labeled D_9 -Pip (F) and L-Lys-4,4,5,5- d_4 (G) to *Psm*-inoculated Col-0 plants results, in addition to natural NHP (m/z 172), in the formation of D_9 -labeled NHP (m/z 181) (F) and D_4 -labeled NHP (m/z 176) (G), respectively. GC-MS analyses after sample derivatization by trimethylsilylation.

(H–J) Mass spectra with indicated M^+ ions and plausible fragmentation patterns of bis-trimethylsilylated NHP (**1b**) (H), D_9 -NHP (I), and D_4 -NHP (J). The spectra are derived from the substance peaks depicted in (E)–(G).

See also Figures S3 and S4.

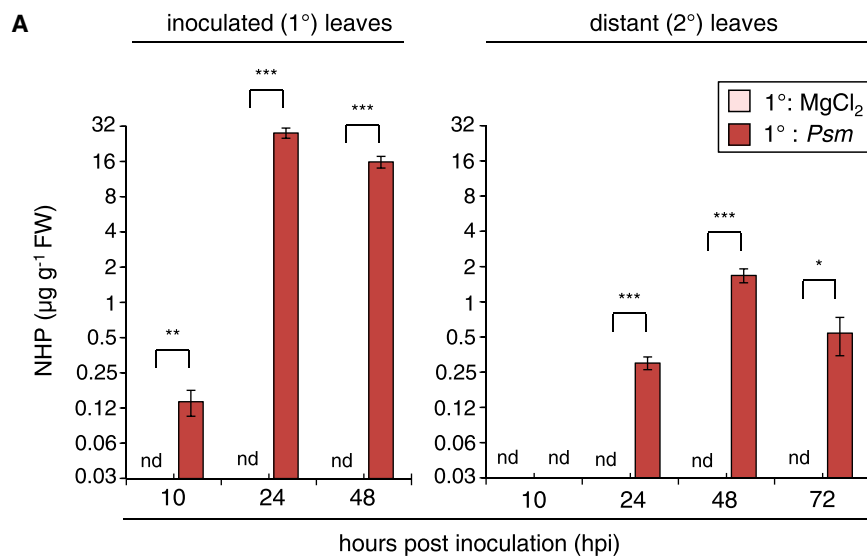
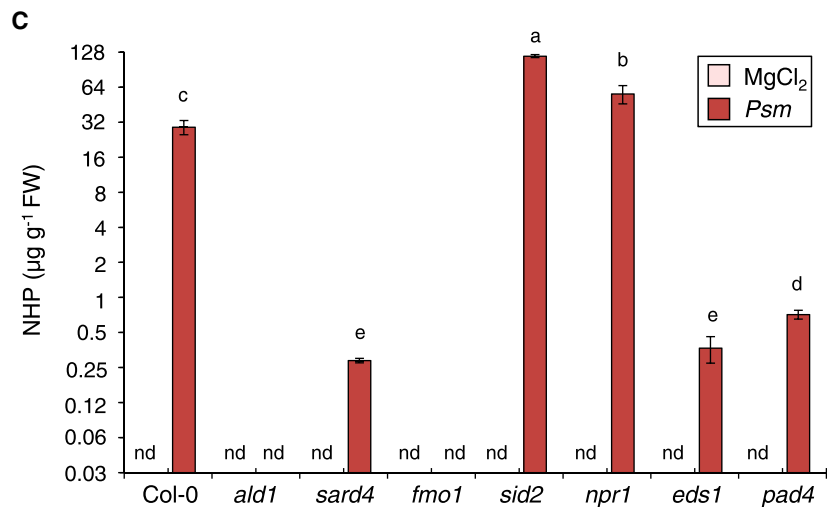
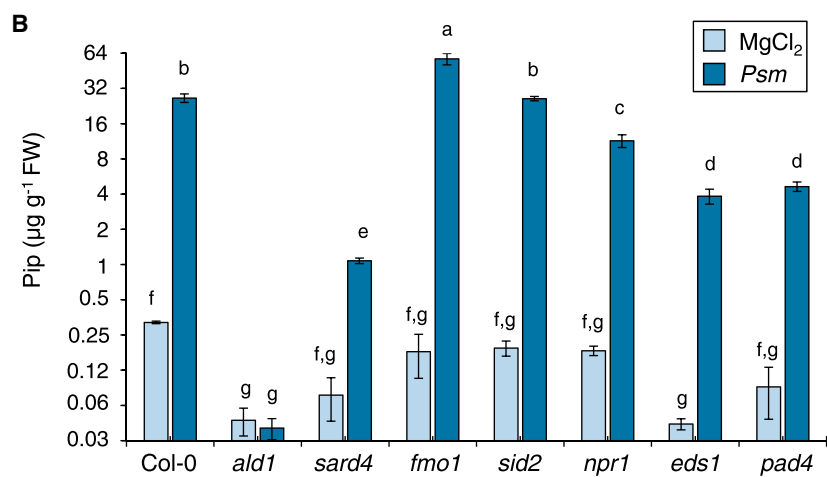


Figure 3. NHP Accumulates Systemically in the *Arabidopsis* Foliage at the Onset of SAR

(A) Levels of N-hydroxypipicolinic acid ($\mu\text{g g}^{-1}$ leaf fresh weight [FW]) in *Psm*-inoculated or mock-inoculated (MgCl_2 -infiltrated) 1° leaves and in distant (2°) leaves of Col-0 plants at different times after inoculation. Data represent the mean \pm SD of at least three biological replicates. Asterisks denote significant differences between *Psm*- and mock-treated samples (* $p < 0.05$; ** $p < 0.01$; *** $p < 0.001$; two-tailed t test). NHP was not detected (nd) in control samples (detection limit $\sim 0.01 \mu\text{g g}^{-1}$ FW). The y-axes are presented in logarithmic (\log_2) scaling.

(B and C) Levels of Pip (B) and NHP (C) in *Psm*-inoculated and 10 mM MgCl_2 -infiltrated leaves of Col-0 and different mutant plants at 24 hpi. Different letters denote significant differences ($p < 0.05$, ANOVA and post hoc Tukey HSD test). The y-axes have \log_2 scaling. See also Figure S5.



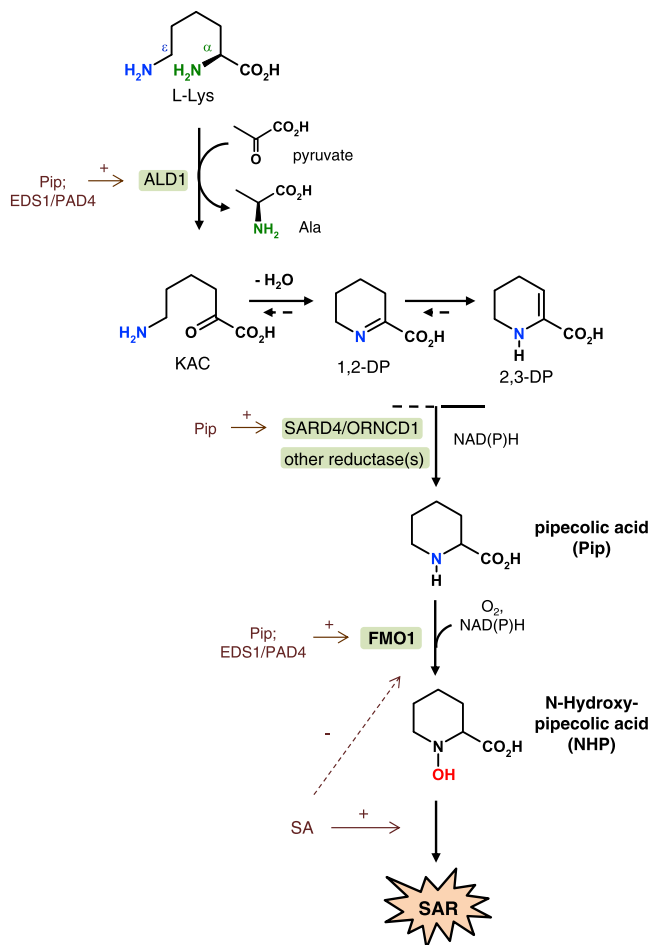


Figure 4. The NHP Biosynthetic Pathway Defines a Novel, Pathogen-Inducible Route of L-Lys Catabolism in Plants Essential for SAR

The L-Lys α -aminotransferase ALD1 catalyzes the generation of ϵ -amino- α -ketocaproic acid (KAC), followed by dehydrative cyclization to 1,2-dehydri-pipecolic acid (1,2-DP) and isomerization to the *in planta* detectable enamine 2,3-DP. SARD4/ORNCD1 and other reductase activities then reduce DP intermediates to Pip. Finally, Pip is N-hydroxylated by FMO1 to NHP whose accumulation is necessary for SAR. The pathway is positively regulated by Pip and EDS1/PAD4 signaling at the transcriptional level. SA cooperates with NHP in acquired resistance induction and dampens the surplus accumulation of NHP.

half of the maximum value in the attacked leaves whereas Pip further accumulated, revealing a divergence in the accumulation patterns of NHP and Pip at later stages of infection in the 1^o leaf (Figure S5A).

The SAR response in the distal, 2^o leaves of *Psm*-inoculated Col-0 plants inoculated in 1^o leaves with *Psm* starts to develop not earlier than 24 hpi and is established at 48 hpi under the applied experimental conditions (Návarová et al., 2012). In accordance with our previous findings, both Pip and SA accumulated in the 2^o leaves at 48 hpi but not yet at 24 hpi in the present time course analyses (Figure S5A). By contrast, NHP started to accumulate already at 24 hpi and reached a maximum at 48 hpi (1.5 to 2 $\mu\text{g g}^{-1}$ FW) in the 2^o leaves (Figure 3A). Thus,

NHP is biosynthesized to high amounts in the 1^o-inoculated leaves in response to *Psm* attack and accumulates in the 2^o leaves at the very onset of SAR.

NHP Generation in *Arabidopsis* Completely Depends on the Biosynthetic Genes *ALD1* and *FMO1* and Is Boosted by the Immune Regulators *EDS1* and *PAD4*

We next examined the *Psm*-induced generation of NHP and Pip in different *Arabidopsis* mutants with defects in key immune regulatory genes in inoculated leaves at 24 and 48 hpi (Figures 3B, 3C, and S5B). The accumulation of both NHP and Pip was absent in the *ald1* mutant and markedly reduced in the dehydri-pipecolic acid reductase mutant *sard4* (Figures 3B and 3C). By contrast, *fmo1* strongly generated Pip at the sites of *Psm* inoculation, but was completely defective in NHP biosynthesis (Figures 3B and S5B). This suggests that FMO1 constitutes the single pipecolic acid N-hydroxylase in *Arabidopsis*. Together with the *in vitro* and isotope-labeling studies (Figures 2, S3, and S4) (Hartmann et al., 2017), the phenotypes of the *ald1*, *sard4*, and *fmo1* mutants show that NHP is synthesized upon pathogen-inoculation from L-Lys by a reaction sequence that involves three enzymatic steps: α -transamination of L-Lys by the aminotransferase ALD1, subsequent reduction of the intermediate 2,3-DP to Pip by SARD4 (and other reductive activities), and finally N-hydroxylation of Pip by FMO1 (Figure 4).

We next examined Pip and NHP levels in *Psm*-inoculated plants defective in *enhanced disease susceptibility1* (*EDS1*) and *phytoalexin-deficient4* (*PAD4*), which encode key regulators of *Arabidopsis* basal immunity that are required for the proper induction of defense gene expression and SA biosynthesis (Bartsch et al., 2006). While Pip accumulated to ~15% of the wild-type levels in the leaves of *pad4* or *eds1* knockout plants at 24 hpi, NHP levels only accounted for ~2% of the wild-type levels in both mutants at this stage of infection (Figures 3B and 3C). Similarly reduced levels of Pip and NHP were observed at 48 hpi (Figure S5B). The biosynthesis of NHP is thus tightly controlled by EDS1/PAD4 signaling, evidently at both the levels of Pip generation and Pip hydroxylation. We then asked whether SA is involved in the regulation of NHP production and examined the *Psm*-triggered NHP accumulation in the SA-deficient mutant *sid2* and in the SA-insensitive mutant *npr1*. At 24 hpi, NHP was produced to ~4- and 2-fold higher levels in *sid2* and *npr1* than in the wild-type, respectively (Figure 3C), and further over-accumulated to ~10-fold in *sid2* at 48 hpi (Figure S5B). Therefore, NHP generation does not require functional SA signaling, but SA modulates the accumulation of surplus NHP appears to operate downstream of Pip biosynthesis (Figure 4), because Pip neither over-accumulated in *sid2* nor in *npr1* (Figures 3B and S5B).

Exogenous NHP Acts as a Potent Inducer of Plant Immunity to Bacterial and Oomycete Infection and Abolishes the Resistance Defects of *fmo1*

The biochemical function of FMO1 as an NHP-generating pipecolic acid N-hydroxylase, the concurrent key role of FMO1 in SAR and Pip-mediated immune responses, and the substantial systemic accumulation of NHP in the SAR-induced wild-type

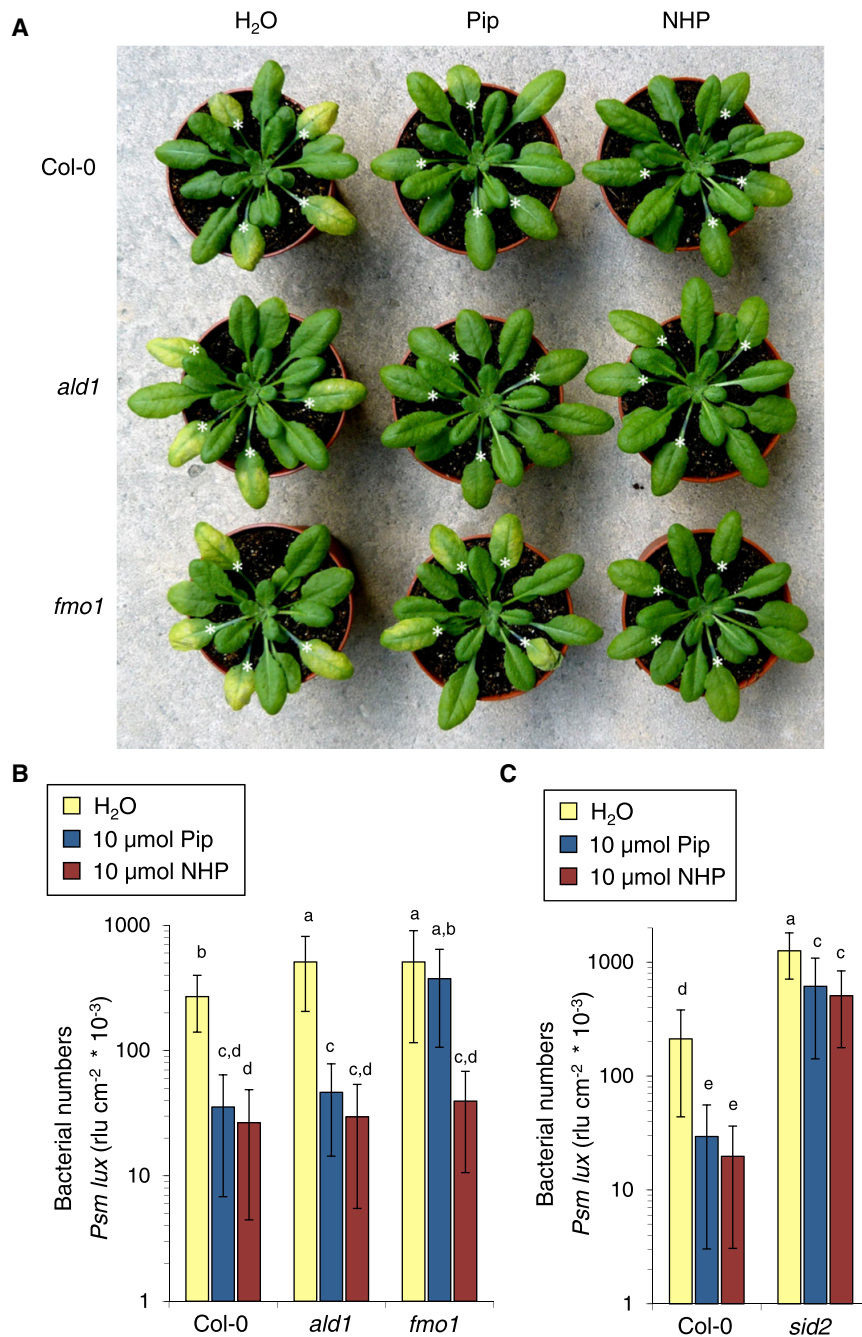


Figure 5. Exogenous NHP Is a Potent Inducer of *Arabidopsis* Immunity to *P. syringae* Infection and Overrides the Acquired Resistance Defect of the NHP-Deficient *fmo1* Mutant

(A) 5-week-old Col-0, *ald1*, or *fmo1* plants were pre-treated with 10 μmol of Pip (middle), 10 μmol of NHP (right), or not pre-treated (left). One day later, four leaves of each plant (white asterisks) were inoculated with *Psm lux* ($OD_{600nm} = 0.001$). Representative plants were photographed 72 hr post inoculation (hpi).

(B and C) Bacterial numbers were assessed at 60 hpi with the bioluminescent *Psm lux* strain and expressed as relative light units (rlu) per cm² leaf area. Data represent the mean ± SD of at least 20 leaf replicates from 6 to 7 different plants. Different letters denote significant differences ($p < 0.005$, ANOVA and post hoc Tukey HSD test). Experiments with Col-0, *ald1* and *fmo1* (B), and Col-0 and *sid2* (C) are shown.

numbers in leaves (Figure 5A). Leaves of *ald1* and *fmo1* mutants thereby hosted significantly higher amounts of bacteria than the leaves of the Col-0 wild-type at 60 hpi (Figure 5B). The *Hpa*-inoculated leaves of non-pre-treated Col-0 showed extensive areas of whitish downy mildew symptoms (Figures 6A and S6). At the microscopic level, leaves were pervaded with intercellular hyphae (IH) which we visualized by Trypan blue staining (Figures 6B and 7A, image I). A quantitative assessment determined average lengths of ~500 μm per cm² leaf area for the IH at 7 dpi (Figure 7B). Moreover, sporangio-phores (SP) densely developed on the leaf surfaces (Figures 7A, image II, and 7B), and the majority of leaves were covered with several hundreds of oospores (OS) per cm² leaf area (Figures 7A, image III, and 7B). The macroscopically visible mildew symptoms were generally more pronounced on the leaf surfaces of untreated *ald1* and *fmo1* plants than on the leaves of the wild-type (Figures 6A and S6). Moreover, IH were more extended and the numbers of SP and

suggested a critical role for NHP in plant acquired resistance to pathogen infection. To verify this hypothesis, we supplied individual plants with doses of 10 μmol Pip, 10 μmol NHP, or water (control treatment) and assessed resistance against leaf infection by a compatible, bioluminescent *Psm* strain (*Psm lux*) or by the virulent oomycete *Hpa* isolate Noco2 (Fan et al., 2008; Bartsch et al., 2006).

The *Psm*-inoculated leaves of the non-pre-treated Col-0, *ald1*, and *fmo1* control plants exhibited pronounced chlorotic disease symptoms after 3 days accompanied with high bacterial

OS were higher on the leaves of the two mutants than on the Col-0 leaves (Figure 7C). Together, this indicates that proper basal resistance of *Arabidopsis* to bacterial and oomycete infection is dependent on functional *ALD1* and *FMO1* and therefore on intact NHP biosynthesis.

The pre-treatment of plants with Pip strongly increased resistance of wild-type and *ald1* plants to both *Psm* and *Hpa*. Chlorotic leaf symptoms were suppressed in *Psm*-inoculated Col-0 and *ald1* leaves, and the leaves of Pip-treated plants had 10-fold lower levels of bacteria compared with the leaves of

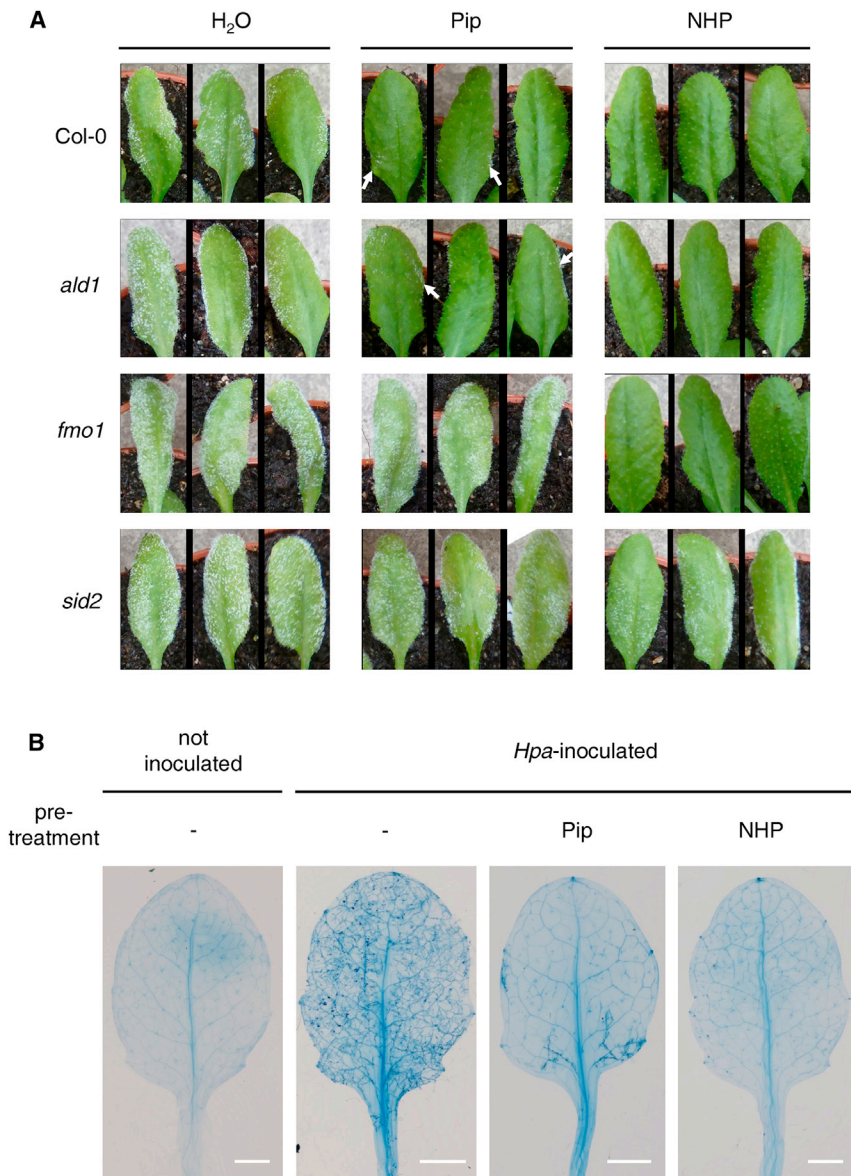


Figure 6. Exogenous NHP Effectively Protects *Arabidopsis* from Invasion by the Oomycete *Hyaloperonospora arabidopsidis* and Confers, in Contrast to Pip, Acquired Resistance to *fmo1*

(A) 4-week-old *Arabidopsis* Col-0, *ald1*, *fmo1*, and *sid2* plants were pretreated with Pip (middle) or NHP (right). Non-pretreated control plants (left) and pretreated plants were spray-inoculated with a suspension of sporangia ($5 \times 10^4 \text{ mL}^{-1}$) of *Hyaloperonospora arabidopsidis* (*Hpa*) isolate Noco2. Leaves of plants were photographed 7 days after inoculation. NHP-pretreated Col-0, *ald1*, and *fmo1* plants appear completely symptom-free, whereas non-pretreated plants show extensive areas of whitish downy mildew symptoms. Pip-treated Col-0 and *ald1* plants only sporadically show small areas of visible mildew symptoms (arrows). Non-pretreated and Pip-pretreated *fmo1* plants show similar, heavy disease symptomology.

(B) Overview shots of representative Trypan-blue-stained leaves of *Hpa* Noco2-inoculated *Arabidopsis* Col-0 plants after supplementation with 10 mL H₂O (–), 10 μmol Pip (Pip), or 10 μmol NHP (NHP). Leaves were harvested and stained at 7 dpi. A non-inoculated, Trypan blue-stained leaf is shown for comparison. Scale bar, 2 mm. See also Figure S6.

control plants at 60 hpi (Figures 5A and 5B). Following *Hpa*-inoculation, Pip-pre-treated Col-0 plants were largely symptom-free at the macroscopic level and only occasionally contained small areas of visible mildew symptoms (Figures 6A and S6). Moreover, the average length of IH growing inside leaves was strongly reduced (Figure 7B). Unlike naive plants, ~60% of IH in leaves of the Pip-treated Col-0 plants were closely encased by dead host cells (Figures 6B and 7A, image IV), a plant defense reaction to *Hpa* previously designated as trailing necrosis (Uknes et al., 1992). In addition, Pip-pre-treatment greatly diminished the occurrence of SP on leaves and fully prevented the development of OS at 7 dpi (Figures 6B and 7B). The same protective effect of exogenous Pip was also observed for *ald1*, although the level of Pip-induced acquired resistance to *Hpa* seemed somewhat lower for *ald1* than for Col-0 (Figures 6A, 7C, and S6). By

contrast, *fmo1* plants remained susceptible to infection by *Psm* and *Hpa* after Pip-treatment, indicating that the *fmo1* defect in acquired resistance to both pathogen types was not complemented by exogenous Pip (Figures 5A, 5B, 6A, 7C, and S6).

Significantly, pre-treatment of plants with NHP strongly increased resistance to bacterial and oomycete infection in Col-0, *ald1*, and *fmo1*. NHP feeding abolished the chlorotic symptom development normally observed upon *Psm* infection and attenuated bacterial growth by at least one order of magnitude in all the genotypes (Figures 5A and 5B). Moreover, Col-0 plants pre-treated with NHP before

Hpa inoculation were completely free of mildew symptoms at 7 dpi (Figures 6A, 7C, and S6). Trypan blue-stained leaves of NHP-supplemented and *Hpa*-inoculated plants generally resembled stained leaves of non-inoculated plants (Figure 6B), except that sporadically, microscopic lesions consisting of one or a few dead cells were discernable. These were reminiscent of highly localized hypersensitive response (HR) lesions (Figure 7A, image V). In addition, the invasive growth of *Hpa* inside leaves was effectively blocked by NHP pre-treatment. The formation of IH was fully prohibited in ~70% of the examined leaves, while in the remaining 30%, an occasional occurrence of very short hyphae inside leaves (length between 0.5 to 2 mm cm^{-2}) was observed (Figure 7B). These rudimentary hyphae were usually accompanied with a trailing necrotic reaction of the plant (Figure 7B). Further, the NHP-pre-treatment completely inhibited

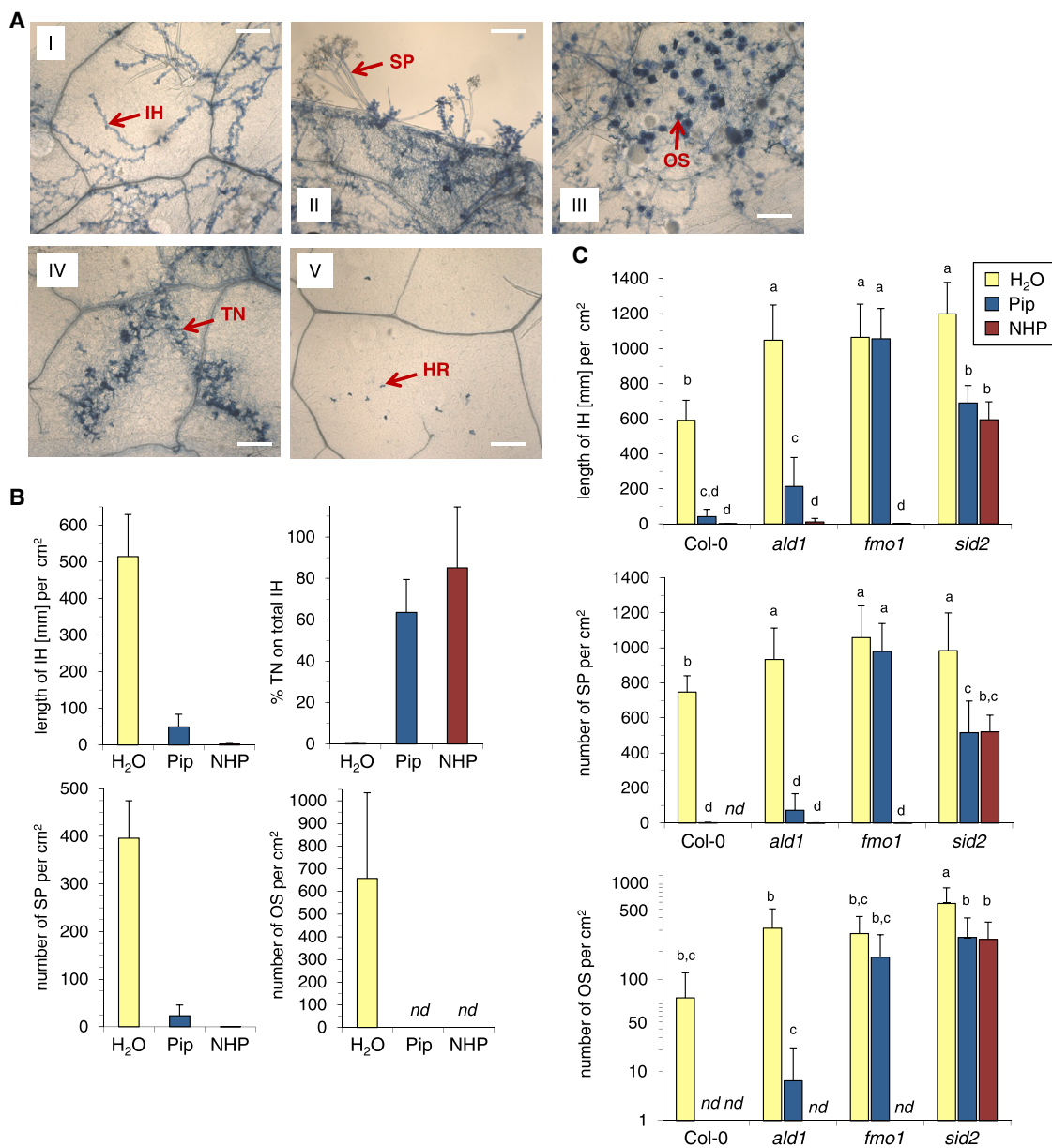


Figure 7. Quantitative Assessment of Disease Stages and Resistance Characteristics in *Hpa*-Infected Plants

(A) Micrographs of Trypan-blue-stained leaves of *Hpa* Noco2-inoculated *Arabidopsis* Col-0 plants at 7 dpi, representing typical disease stages (I, II, III) or resistance phenotypes (IV, V). I: free intercellular hyphae (IH) inside leaf; II: sporangiophores (SP) on leaf surface; III: oospore (OS) formation on leaf; IV: trailing necrosis (TN) of plant cells encasing hyphae; V: symptom-free leaf with sporadically occurring, highly localized hypersensitive response (HR) lesions. Scale bar, 200 μ m.

(B) Quantitative assessment of different disease stages (IH, SP, OS) and resistance characteristics (TN) of control-, Pip-pretreated or NHP-pretreated Col-0 plants at 7 d post *Hpa* inoculation. Top left: length of total (sum of free and TN-associated) IH (mm) per cm² leaf area. Top right: length of IH associated with TN related to the length of total IH (in %). Bottom left: number of SP per cm² leaf area. Bottom right: number of OS per cm² leaf area. Bars represent means \pm SD of 10 leaf replicates.

(C) Quantitative assessment of IH, SP, and OS of *Hpa*-inoculated Col-0, *ald1*, *fmo1*, and *sid2* plants in a further experiment. Different letters denote significant differences ($p < 0.05$, ANOVA and post hoc Tukey HSD test).

See also Figure S6.

the development of SP and OS on Col-0 leaves (Figure 7B). Therefore, NHP functions as a potent inducer of acquired resistance to *P. syringae* and *H. arabidopsidis* infection in *Arabidop-*

sis. Importantly, exogenous NHP complemented the acquired resistance defect of the NHP biosynthesis mutant *fmo1*. These resistance phenotypes and the biochemical function of FMO1

as a pipercolate N-hydroxylase demonstrate that the FMO1-mediated conversion of Pip to NHP and the subsequent accumulation of NHP are critical for the acquired resistance response in *Arabidopsis* (Figures 2–7). The previously described resistance effects of Pip are thus attributable to the accumulation of NHP which is generated from Pip by FMO1.

To analyze the significance of SA signaling for the NHP-mediated immune response, we examined the effects of exogenous NHP on resistance to *Psm* and *Hpa* in the SA biosynthesis-defective *sid2* mutant. *Sid2* is substantially compromised in basal resistance to *P. syringae* and *Hpa* infection (Nawrath and Métraux, 1999). Consistently, we observed significantly higher bacterial growth and heavier oomycete infection in the leaves of non-pretreated *sid2* plants compared to Col-0 plants. Both Pip- and NHP-pre-treatment significantly reduced the growth of *Psm* and noticeably moderated downy mildew symptoms and *Hpa* invasive structures in the leaves of *sid2*. However, these resistance effects were markedly lower in *sid2* than in Col-0 (Figures 5C, 6A, 7C, and S6). Thus, the full potential of NHP in mediating plant acquired resistance is only realized in association with an intact SA biosynthetic pathway although an SA-independent component of NHP-inducible immunity also exists.

DISCUSSION

In the current study, we have identified the N-hydroxylated amino acid N-hydroxypipercolic acid as an endogenously produced *Arabidopsis* metabolite with a critical role in plant acquired resistance to pathogen infection (Figure 4). NHP was not detected in unstressed, naive plants but strongly accumulated in leaves of *P. syringae*-challenged plants (Figure 3). Until now, N-hydroxylated substances have rarely been described as plant-derived natural products. While oximes that contain hydroxylated sp²-hybridized nitrogens are characterized intermediates in the biosynthesis of glucosinolates and cyanogenic glucosides (Wittstock and Halkier, 2000), hydroxylated, sp³-nitrogen-containing amines or amino acids such as NHP have, to our knowledge, not been reported before as natural plant constituents. However, bacteria and fungi use N-hydroxylating monooxygenases to hydroxylate the primary amino groups in the side chains of L-Lys and L-Orn, as well as in some primary aliphatic diamines such as putrescine to generate respective N-hydroxy derivatives (Olucha and Lamb, 2011). Further, larvae of the European cinnabar moth *Tyria jacobaeae* specifically convert toxic pyrrolizidine alkaloids ingested by feeding on their host plant *Senecio jacobaea* into non-toxic N-oxides via the FMO senecionine N-oxygenase (Naumann et al., 2002).

The biosynthesis of NHP in *Arabidopsis* proceeds by the FMO1-mediated N-hydroxylation of the secondary amino group in the piperidine ring of Pip (Figures 2 and 4). *Arabidopsis* FMO1 thus catalyzes a biochemical N-hydroxylation reaction similar to those of bacterial N-hydroxylating monooxygenases. The substrates and the biochemistry for the characterized plant FMOs from clade II and III are different from those of the clade I-associated FMO1. *Arabidopsis* FMOs from clade III S-oxygenate methylthioalkyl to methylsulfinylalkyl moieties in the biosynthesis of Met-derived glucosinolates (Li et al., 2008). Similarly, an *Allium sativum* clade III FMO mediates the S-oxygenation reaction

required for the biosynthesis of the L-Cys-derived sulfoxide alliin (Yoshimoto et al., 2015). By contrast, the clade II YUCCAs catalyze the oxidative decarboxylation of indole-3-pyruvate to the plant hormone IAA (Mashiguchi et al., 2011), a reaction that apparently does not involve a direct oxygenation of a heteroatom. A common characteristic of all characterized plant FMOs is that they have endogenous substrates and catalyze biochemical reactions within defined metabolic pathways. By contrast, the five human FMOs mediate the oxidative degradation of a broad range of heteroatom-containing xenobiotics (Rossner et al., 2017).

L-Lys catabolism in plants comprises the saccharopine pathway that generates α -amino adipic acid and the lysine decarboxylase-catalyzed biosynthesis of the diamine cadaverine (Galili et al., 2001; Bunsupa et al., 2012; Zeier, 2013). Our work has now uncovered a pathogen-inducible L-Lys catabolic pathway that culminates in the accumulation of NHP (Figures 2, 3, and 4). Pathway activation already starts at the level of the precursor amino acid Lys, whose leaf levels rise in response to pathogens (Návarová et al., 2012). In a first enzymatic step, the α -NH₂-group of L-Lys is transferred to an acceptor oxoacid in an aminotransferase reaction catalyzed by ALD1 (Figure 4). The resulting *in planta* detectable product is 2,3-DP, which is formed from the initial Lys transamination product ϵ -amino- α -ketocaproic acid (KAC) by dehydrative cyclization and subsequent keto-enol tautomerization of 1,2-DP (Figure 4). Although recombinant ALD1 protein accepts several amino acids other than L-Lys as *in vitro* substrates, *in planta* analyses suggest that the α -transamination of L-Lys to 2,3-DP is the sole *in vivo* function of ALD1 (Hartmann et al., 2017). In a second enzymatic step, the Rossmann-fold-containing protein SARD4 contributes to the NAD(P)H-dependent reduction of dehydropipercolic acid intermediates to Pip (Hartmann et al., 2017) (Figure 4). Subcellular localization studies with plants expressing ALD1- and SARD4-reporter proteins suggest that Pip, like the precursor amino acid L-Lys, is synthesized in plastids (Sharma et al., 2013; Cecchini et al., 2015).

We demonstrated here by both *in vitro* and *in planta* analyses that the final enzymatic step in the biosynthesis of NHP is the FMO1-catalyzed, NAD(P)H- and O₂-dependent N-hydroxylation of Pip (Figures 2, 3, and 4). The biosynthetic scheme from L-Lys to NHP depicted in Figure 4 is fully supported by our plant feeding experiments with L-Lys-4,4,5,5-d₄, L-Lys-6-¹³C, ϵ -¹⁵N, and D₉-Pip (Figures 2 and S4) (Hartmann et al., 2017). The NHP biosynthetic pathway has inducible character, because expression of *ALD1*, *SARD4*, and *FMO1* is strongly enhanced in response to pathogen attack in both inoculated and systemic leaves (Song et al., 2004; Mishina and Zeier, 2006; Hartmann et al., 2017). Interestingly, all the NHP biosynthetic genes are upregulated by elevated Pip (Figure S2), indicating that the accumulating precursor Pip amplifies NHP biosynthesis by both feedback and feedforward stimulation at the transcriptional level (Figure 4). In addition, NHP generation is tightly regulated by the EDS1/PAD4 immune regulatory node (Figures 3C and S5B). Consistently, previous studies revealed that upregulation of the NHP biosynthetic genes *ALD1* and *FMO1* is positively stimulated by *EDS1* and *PAD4* (Figure 4) (Song et al., 2004; Bartsch et al., 2006; Mishina and Zeier, 2006; Návarová et al., 2012).

Furthermore, it is likely that the transcriptional control of NHP biosynthesis also involves the two transcription factors SARD1 and CBPG60, because chromatin immunoprecipitation analyses suggested that they target the promoters of *ALD1* and *FMO1* (Sun et al., 2015).

The present study shows that elevated Pip is sufficient to induce a set of ~700 *Arabidopsis* genes, many of which are regulatory elements of SAR and plant basal immunity. The transcriptional response to Pip is an integral part of SAR-associated transcriptional reprogramming (Figures 1, S1, and S2) (Bernsdorff et al., 2016). Significantly, all of the hitherto known responses to Pip, i.e., systemic resistance induction, establishment of defense priming, and direct induction of SAR gene expression, are dependent on functional *FMO1* (Figure 1A) (Návarová et al., 2012; Gruner et al., 2013; Bernsdorff et al., 2016). The defense phenotypes of *fmo1* and the now elucidated biochemical function of *FMO1* as NHP-generating pipecolate hydroxylase indicate that NHP is the actual mediator of the immune responses previously assigned to Pip (Návarová et al., 2012). This is verified by our finding that exogenous NHP—but not Pip—fully restores the capacity to acquire resistance toward *P. syringae* and *Hpa* attack in the NHP-deficient *fmo1* mutant (Figures 5–7 and S6). Thus, NHP constitutes a critical metabolic regulator of SAR in *Arabidopsis*.

The establishment of SAR is dependent on or positively influenced by a set of signal-active metabolites and regulatory proteins (reviewed in Shah and Zeier, 2013). However, the requirement of some of the identified SAR regulators seems to depend on environmental variables and laboratory conditions. Since the initial discoveries of *ALD1* and *FMO1* as important SAR players (Song et al., 2004; Mishina and Zeier, 2006), numerous studies from different laboratories have confirmed the indispensability of these genes for SAR induction under variable settings (Jung et al., 2009; Liu et al., 2011; Návarová et al., 2012), including an unbiased mutant screen for SAR-related genes (Jing et al., 2011). These findings indicate that the NHP biosynthetic pathway constitutes a core and indispensable element of SAR.

SAR equips plants with broad-spectrum immunity to a range of different biotrophic and hemibiotrophic phytopathogens (Fu and Dong, 2013). Accordingly, we have established that NHP effectively mediates acquired resistance to pathogen types with distinct phylogenetic origin and inherently different mode of infection, i.e., the hemibiotrophic bacterium *P. syringae* and the biotrophic oomycete *Hpa*. It is reasonable to assume that the above-mentioned direct induction of defense-related gene expression and the establishment of a primed state significantly contribute to these protective effects, because the responses strictly depend on Pip accumulation and functional *FMO1* (Figure 1) (Bernsdorff et al., 2016).

Strikingly, the NHP pre-treatment converted the compatible *Hpa*-*Arabidopsis* interaction that is associated with massive invasive growth and the development of numerous epiphytic reproductive oomycete structures virtually into a symptomless, incompatible interaction (Figures 6, 7, and S6). The occurrence of scattered, microscopic HR lesions in the leaves of NHP-pre-treated and *Hpa*-inoculated plants suggests that highly localized hypersensitive cell death events, possibly at sites of attempted oomycete penetration, contribute to this strong, NHP-mediated resistance effect (Figure 7A, image V). In the very rare cases in

which short intercellular hyphae developed inside leaves of NHP-pre-treated plants, they were usually surrounded by necrotic plant cells, suggesting that a trailing necrosis reaction had stopped the extension of hyphae very early after oomycete entry into leaves (Figure 7B). This protective effect of NHP to *Hpa* infection is reminiscent of the previously described action of the synthetic resistance enhancer 2,6-dichloroisonicotinic acid (Uknes et al., 1992). Consistent with the here-described function of *FMO1* as NHP synthase, overexpression of *FMO1* in *Arabidopsis* resulted in similar protection to *Hpa* and *P. syringae* infection than NHP-pre-treatment (Koch et al., 2006; Bartsch et al., 2006). *Arabidopsis* lines overexpressing *FMO1* variants in which conserved Gly residues in either the FAD- or NADPH-binding motifs were changed to Ala did not confer enhanced protection, indicating and corroborating our present finding that the enzymatic activity of *FMO1* is required for its role in immunity (Bartsch et al., 2006).

The systemic increase of NHP in the distal leaves of *P. syringae*-inoculated plants starts at the very onset of the SAR response at 24 hpi, already before systemic Pip and SA accumulation is observable (Figures 3A and S5A). These early systemic rises in NHP might be caused by the translocation from 1°-inoculated leaves, in which the compound accumulates to high levels (Figure 3), to the distant 2° leaves. Alternatively, rapid systemic signaling processes might induce early expression of *FMO1* in the 2° leaves, and *FMO1* in turn catalyzes the hydroxylation of Pip that is present to low basal levels also in non-induced plants (Figure S5). For example, reactive oxygen species (ROS) have been implicated in rapid systemic defense signal transduction and SAR (Alvarez et al., 1998; Dubiella et al., 2013; Wang et al., 2014), and ROS-generating treatments proved sufficient to trigger *FMO1* expression in *Arabidopsis* leaves (Olszak et al., 2006). Future studies on the function of NHP in long-distance defense signaling transduction will likely further improve the mechanistic understanding of SAR.

Previous genetic analyses in *Arabidopsis* indicated that *ALD1* and *FMO1* mediate plant resistance by partially SA-independent signaling modes (Song et al., 2004; Bartsch et al., 2006; Zhang et al., 2008). Moreover, our recent study suggested that a Pip/*FMO1* regulatory module mediates SAR by both SA-independent and SA-dependent activation pathways (Bernsdorff et al., 2016). Consistently, Pip/*FMO1*-derived NHP triggered a significant acquired resistance response in the SA-deficient *sid2* mutant. However, NHP clearly required inducible SA biosynthesis to provide strong protection against *P. syringae* or *Hpa* invasion, suggesting a functional interplay of NHP and SA in resistance induction (Figures 5C, 6A, and 7C). Moreover, our metabolite analyses suggest that increased SA levels attenuate the pathogen-induced accumulation of NHP to excess levels at the stage of Pip to NHP conversion (Figures 3B, 4, and S5B). In line with this assumption, SA-deficient *sid2* shows a stronger pathogen-inducible *FMO1* expression than the SA accumulating wild-type (Bernsdorff et al., 2016). The molecular structures of NHP and SA resemble each other, particularly with respect to the presence of similarly arranged carboxylic acid and hydroxyl functional groups (Figure S4F). Whether this structural resemblance determines the biological function of and the interplay between NHP and SA in plant immunity remains to be determined.

In conclusion, our work has identified a pathogen-inducible L-Lys catabolic pathway in *Arabidopsis* that generates N-hydroxypipecolic acid, a previously undescribed plant metabolite with a central function in SAR. Because the NHP precursor Pip is widely distributed in angiosperms and FMO1 orthologs exist in other plant species (Figure S7), we consider it likely that L-Lys catabolism to NHP constitutes a common plant metabolic defense pathway. Exogenous application of low doses of NHP confers effective protection to *Arabidopsis* against attack by pathogen types with inherently different modes of infection. Our study therefore promises to contribute to the development of natural product-based plant protection strategies.

STAR★METHODS

Detailed methods are provided in the online version of this paper and include the following:

- **KEY RESOURCES TABLE**
- **CONTACT FOR REAGENT AND RESOURCE SHARING**
- **EXPERIMENTAL MODEL AND SUBJECT DETAILS**
 - *Arabidopsis*
 - *Pseudomonas*
 - *Hyaloperonospora arabidopsidis* (Downy Mildew)
- **METHOD DETAILS**
 - GC-MS analysis of metabolites
 - GC-FTIR analysis of metabolites
 - Chemical synthesis of N-hydroxypipecolic acid
 - Plant treatments with Pip and NHP
 - Assessment of plant resistance to *P. syringae*
 - Assessment of plant resistance to Hpa
 - Trypan Blue Staining
 - Microscopic analysis of Hpa infection
 - Treatment with Isotope-Labeled Metabolites
 - Cloning of FMO1
 - Purification of recombinant FMO1 enzyme
 - FMO1 activity assays
 - Genome-Wide Analyses of the Plant Transcriptional Response to Pip
 - Phylogenetic analysis of potential FMO1 orthologs
- **QUANTIFICATION AND STATISTICAL ANALYSIS**
- **DATA AND SOFTWARE AVAILABILITY**

SUPPLEMENTAL INFORMATION

Supplemental Information includes seven figures and two tables and can be found with this article online at <https://doi.org/10.1016/j.cell.2018.02.049>.

ACKNOWLEDGMENTS

We thank Jane Parker for providing the *Hpa* Noco2 strain, Steffen Köhler (Center for Advanced Imaging, HHU Düsseldorf) for support with respect to the acquisition of leaf overview images, and Laura Rose for proofreading the manuscript. This work was supported by the German Research Foundation (DFG grant ZE467/6-1).

AUTHOR CONTRIBUTIONS

M. Hartmann, V.R.-D., D.K., N.S., S.S., and J.Z. performed the bacterial assays and metabolite analyses. M. Hartmann and D.K. conducted the biochem-

ical assays. T.Z. implemented and performed, with assistance of M. Hohmann, the oomycete infection experiments. A.B. and F.B. conducted the RNA-seq analyses. J.Z. evaluated the expression data. T.H. and C.G. chemically synthesized NHP. M. Hartmann assisted J.Z. in manuscript preparation and design of experiments. J.Z. secured funding, conceived the research, and wrote the manuscript.

DECLARATION OF INTERESTS

The authors declare no competing interests.

Received: November 15, 2017

Revised: January 16, 2018

Accepted: February 20, 2018

Published: March 22, 2018

REFERENCES

- Alvarez, M.E., Pennell, R.I., Meijer, P.-J., Ishikawa, A., Dixon, R.A., and Lamb, C. (1998). Reactive oxygen intermediates mediate a systemic signal network in the establishment of plant immunity. *Cell* 92, 773–784.
- Bartsch, M., Gobbato, E., Bednarek, P., Debey, S., Schultze, J.L., Bautor, J., and Parker, J.E. (2006). Salicylic acid-independent ENHANCED DISEASE SUSCEPTIBILITY1 signaling in *Arabidopsis* immunity and cell death is regulated by the monooxygenase FMO1 and the Nudix hydrolase NUDT7. *Plant Cell* 18, 1038–1051.
- Benjamini, Y., and Hochberg, Y. (1995). Controlling the false discovery rate: a practical and powerful approach to multiple testing. *J. R. Stat. Soc. Series B Stat. Methodol.* 57, 289–300.
- Bernsdorff, F., Döring, A.-C., Gruner, K., Schuck, S., Bräutigam, A., and Zeier, J. (2016). Pipecolic acid orchestrates plant systemic acquired resistance and defense priming via salicylic acid-dependent and -independent pathways. *Plant Cell* 28, 102–129.
- Bunsupa, S., Katayama, K., Ikeura, E., Oikawa, A., Toyooka, K., Saito, K., and Yamazaki, M. (2012). Lysine decarboxylase catalyzes the first step of quinolizidine alkaloid biosynthesis and coevolved with alkaloid production in leguminosae. *Plant Cell* 24, 1202–1216.
- Cecchini, N.M., Jung, H.W., Engle, N.L., Tschaplinski, T.J., and Greenberg, J.T. (2015). ALD1 regulates basal immune components and early inducible defense responses in *Arabidopsis*. *Mol. Plant Microbe Interact.* 28, 455–466.
- Dereeper, A., Guignon, V., Blanc, G., Audic, S., Buffet, S., Chevenet, F., Dufayard, J.-F., Guindon, S., Lefort, V., Lescot, M., et al. (2008). Phylogeny.fr: robust phylogenetic analysis for the non-specialist. *Nucleic Acids Res.* 36, W465–9.
- Ding, P., Rekhter, D., Ding, Y., Feussner, K., Busta, L., Haroth, S., Xu, S., Li, X., Jetter, R., Feussner, I., and Zhang, Y. (2016). Characterization of a pipecolic acid biosynthesis pathway required for systemic acquired resistance. *Plant Cell* 28, 2603–2615.
- Dubiella, U., Seybold, H., Durian, G., Komander, E., Lassig, R., Witte, C.P., Schulze, W.X., and Romeis, T. (2013). Calcium-dependent protein kinase/NADPH oxidase activation circuit is required for rapid defense signal propagation. *Proc. Natl. Acad. Sci. USA* 110, 8744–8749.
- Fan, J., Crooks, C., and Lamb, C. (2008). High-throughput quantitative luminescence assay of the growth in planta of *Pseudomonas syringae* chromosomally tagged with *Photobacterium luminescens luxCDABE*. *Plant J.* 53, 393–399.
- Fu, Z.Q., and Dong, X. (2013). Systemic acquired resistance: turning local infection into global defense. *Annu. Rev. Plant Biol.* 64, 839–863.
- Gallii, G., Tang, G., Zhu, X., and Gakiere, B. (2001). Lysine catabolism: a stress and development super-regulated metabolic pathway. *Curr. Opin. Plant Biol.* 4, 261–266.
- Gruner, K., Griebel, T., Návárová, H., Attaran, E., and Zeier, J. (2013). Reprogramming of plants during systemic acquired resistance. *Front. Plant Sci.* 4, 252.
- Hartmann, M., Kim, D., Bernsdorff, F., Ajami-Rashidi, Z., Scholten, N., Schreiber, S., Zeier, T., Schuck, S., Reichel-Deland, V., and Zeier, J. (2017).

- Biochemical principles and functional aspects of pipelicolic acid biosynthesis in plant immunity. *Plant Physiol.* **174**, 124–153.
- Holub, E.B., Beynon, J.L., and Crute, I.R. (1994). Phenotypic and genotypic characterization of interactions between isolates of *Peronospora parasitica* and accessions of *Arabidopsis thaliana*. *Mol. Plant Microbe Interact.* **7**, 223–239.
- Jing, B., Xu, S., Xu, M., Li, Y., Li, S., Ding, J., and Zhang, Y. (2011). Brush and spray: a high-throughput systemic acquired resistance assay suitable for large-scale genetic screening. *Plant Physiol.* **157**, 973–980.
- Jung, H.W., Tschaplinski, T.J., Wang, L., Glazebrook, J., and Greenberg, J.T. (2009). Priming in systemic plant immunity. *Science* **324**, 89–91.
- Koch, M., Vorwerk, S., Masur, C., Sharifi-Sirchi, G., Olivieri, N., and Schlaich, N.L. (2006). A role for a flavin-containing mono-oxygenase in resistance against microbial pathogens in *Arabidopsis*. *Plant J.* **47**, 629–639.
- Li, J., Hansen, B.G., Ober, J.A., Kliebenstein, D.J., and Halkier, B.A. (2008). Subclade of flavin-monoxygenases involved in aliphatic glucosinolate biosynthesis. *Plant Physiol.* **148**, 1721–1733.
- Liu, P.P., von Dahl, C.C., and Klessig, D.F. (2011). The extent to which methyl salicylate is required for signaling systemic acquired resistance is dependent on exposure to light after infection. *Plant Physiol.* **157**, 2216–2226.
- Mashiguchi, K., Tanaka, K., Sakai, T., Sugawara, S., Kawaide, H., Natsume, M., Hanada, A., Yaeno, T., Shirasu, K., Yao, H., et al. (2011). The main auxin biosynthesis pathway in *Arabidopsis*. *Proc. Natl. Acad. Sci. USA* **108**, 18512–18517.
- Mishina, T.E., and Zeier, J. (2006). The *Arabidopsis* flavin-dependent monooxygenase FMO1 is an essential component of biologically induced systemic acquired resistance. *Plant Physiol.* **141**, 1666–1675.
- Murahashi, S.-I., and Shiota, T. (1987). Short-step synthesis of amino acids and N-hydroxyamino acids from amines. *Tetrahedron Lett.* **28**, 6469–6472.
- Naumann, C., Hartmann, T., and Ober, D. (2002). Evolutionary recruitment of a flavin-dependent monooxygenase for the detoxification of host plant-acquired pyrrolizidine alkaloids in the alkaloid-defended arctiid moth *Tyria jacobaeae*. *Proc. Natl. Acad. Sci. USA* **99**, 6085–6090.
- Návarová, H., Bernsdorff, F., Döring, A.-C., and Zeier, J. (2012). Pipelicolic acid, an endogenous mediator of defense amplification and priming, is a critical regulator of inducible plant immunity. *Plant Cell* **24**, 5123–5141.
- Nawrath, C., and Métraux, J.-P. (1999). Salicylic acid induction-deficient mutants of *Arabidopsis* express *PR-2* and *PR-5* and accumulate high levels of camalexin after pathogen inoculation. *Plant Cell* **11**, 1393–1404.
- Olszak, B., Malinovsky, F.G., Brodersen, P., Grell, M., Giese, H., Petersen, M., and Mundy, J. (2006). A putative flavin-containing mono-oxygenase as a marker for certain defense and cell death pathways. *Plant Sci.* **170**, 614–623.
- Olucha, J., and Lamb, A.L. (2011). Mechanistic and structural studies of the N-hydroxylating flavoprotein monooxygenases. *Bioorg. Chem.* **39**, 171–177.
- Rossner, R., Kaeberlein, M., and Leiser, S.F. (2017). Flavin-containing monooxygenases in aging and disease: Emerging roles for ancient enzymes. *J. Biol. Chem.* **292**, 11138–11146.
- Schindelin, J., Arganda-Carreras, I., Frise, E., Kaynig, V., Longair, M., Pietzsch, T., Preibisch, S., Rueden, C., Saalfeld, S., Schmid, B., et al. (2012). Fiji: an open-source platform for biological-image analysis. *Nat. Methods* **9**, 676–682.
- Schlaich, N.L. (2007). Flavin-containing monooxygenases in plants: looking beyond detox. *Trends Plant Sci.* **12**, 412–418.
- Shah, J., and Zeier, J. (2013). Long-distance communication and signal amplification in systemic acquired resistance. *Front. Plant Sci.* **4**, 30.
- Sharma, S., Shinde, S., and Verslues, P.E. (2013). Functional characterization of an ornithine cyclodeaminase-like protein of *Arabidopsis thaliana*. *BMC Plant Biol.* **13**, 182.
- Song, J.T., Lu, H., McDowell, J.M., and Greenberg, J.T. (2004). A key role for *ALD1* in activation of local and systemic defenses in *Arabidopsis*. *Plant J.* **40**, 200–212.
- Sun, T., Zhang, Y., Li, Y., Zhang, Q., Ding, Y., and Zhang, Y. (2015). ChIP-seq reveals broad roles of SARD1 and CBP60g in regulating plant immunity. *Nat. Commun.* **6**, 10159.
- Uknes, S., Mauch-Mani, B., Moyer, M., Potter, S., Williams, S., Dincher, S., Chandler, D., Slusarenko, A., Ward, E., and Ryals, J. (1992). Acquired resistance in *Arabidopsis*. *Plant Cell* **4**, 645–656.
- Wang, C., El-Shetehy, M., Shine, M.B., Yu, K., Navarre, D., Wendehenne, D., Kachroo, A., and Kachroo, P. (2014). Free radicals mediate systemic acquired resistance. *Cell Rep.* **7**, 348–355.
- Wildermuth, M.C., Dewdney, J., Wu, G., and Ausubel, F.M. (2001). Isochorismate synthase is required to synthesize salicylic acid for plant defence. *Nature* **414**, 562–565.
- Wittstock, U., and Halkier, B.A. (2000). Cytochrome P450 CYP79A2 from *Arabidopsis thaliana* L. Catalyzes the conversion of L-phenylalanine to phenylacetaldoxime in the biosynthesis of benzylglucosinolate. *J. Biol. Chem.* **275**, 14659–14666.
- Yoshimoto, N., Onuma, M., Mizuno, S., Sugino, Y., Nakabayashi, R., Imai, S., Tsuneyoshi, T., Sumi, S., and Saito, K. (2015). Identification of a flavin-containing S-oxygenating monooxygenase involved in alliin biosynthesis in garlic. *Plant J.* **83**, 941–951.
- Zeier, J. (2013). New insights into the regulation of plant immunity by amino acid metabolic pathways. *Plant Cell Environ.* **36**, 2085–2103.
- Zeier, J., Pink, B., Mueller, M.J., and Berger, S. (2004). Light conditions influence specific defence responses in incompatible plant-pathogen interactions: uncoupling systemic resistance from salicylic acid and *PR-1* accumulation. *Planta* **219**, 673–683.
- Zhang, Z., Lenk, A., Andersson, M.X., Gjetting, T., Pedersen, C., Nielsen, M.E., Newman, M.A., Hou, B.H., Somerville, S.C., and Thordal-Christensen, H. (2008). A lesion-mimic syntaxin double mutant in *Arabidopsis* reveals novel complexity of pathogen defense signaling. *Mol. Plant* **1**, 510–527.

STAR★METHODS

KEY RESOURCES TABLE

REAGENT or RESOURCE	SOURCE	IDENTIFIER
Bacterial and Virus Strains		
<i>Pseudomonas syringae</i> pv <i>maculicola</i> strain ES4326 (<i>Psm</i>)	Zeier et al., 2004	N/A
<i>Pseudomonas syringae</i> pv <i>maculicola</i> strain ES4326 carrying the <i>Photobacterium luminescens</i> luxCDABE operon (<i>Psm lux</i>)	Fan et al., 2008	N/A
<i>Hyaloperonospora arabidopsidis</i> isolate Noco2	Jane Parker laboratory, MPIPZ Cologne (Germany)	N/A
<i>Escherichia coli</i> Rosetta 2(DE3)pLysS Competent Cells	Novagen	Cat# 71403
Chemicals, Peptides, and Recombinant Proteins		
Salicylic acid-d ₄ (D ₄ -SA)	Sigma-Aldrich	Cat#S-042-1ML; CAS: 78646-17-0
(Trimethylsilyl) diazomethane solution 2 M in hexane	Sigma-Aldrich	Cat#362832; CAS: 18107-18-1
DL-2-Piperidine-d ₉ carboxylic acid (D ₉ -Pip)	CDN Isotopes	Cat#D-5087; CAS: 790612-94-1
L-Lysine-6- ¹³ C, _ε - ¹⁵ N hydrochloride	Sigma-Aldrich	Cat#607665
L-Lysine-4,4,5,5-d ₄ (D ₄ -Lys) hydrochloride	Sigma-Aldrich	Cat#616192
N-Methyl-N-trimethylsilylfluoroacetamide (MSTFA)	Sigma-Aldrich	Cat#69479; CAS: 24589-78-4
Chlorotrimethylsilane (TCMS)	Sigma-Aldrich	Cat#89595; CAS: 75-77-4
2-hydroxy-cyclohexanecarboxylic acid (2-HCC)	Sigma-Aldrich	Cat#R548480
1-hydroxypiperidine-2-carboxylic acid (NHP)	This paper	N/A
Trypan Blue Dye content > 60 %	Alfa Aesar	Cat#A18600; CAS: 72-57-1
Chloral hydrate	Aldrich	Cat#C8383; CAS: 302-17-0
Critical Commercial Assays		
Phusion High-Fidelity DNA Polymerase	NEB	Cat#M0530L
pET-32b(+) vector	Novagen (MERCK)	Cat#69016-3
His GraviTrap	GE Healthcare	Cat#11-0033-99
HisTALON Gravity Columns	Takara Bio	Cat#635655
PD-10 Desalting Columns (Sephadex G-25)	GE Healthcare	Cat#17085101
Bio-Rad Protein Assay	Bio-Rad	Cat#5000002/5000006
RNeasy plant extraction kit	QIAGEN	Cat#74904
TruSeq RNA Sample Prep Kit v2	Illumina	Cat#RS-122-2001/2
Deposited Data		
Sequence data; Genome-wide analyses of the transcriptional response to Pip in <i>Arabidopsis thaliana</i>	This paper	https://www.ebi.ac.uk/arrayexpress/experiments/E-MTAB-6243/
Experimental Models: Organisms/Strains		
Col-0 (<i>A. thaliana</i> accession)	NASC	N1092
T-DNA mutant line of <i>A. thaliana</i> (insertion in At2g13810) (<i>ald1</i>)	NASC; Návarová et al., 2012	SALK_007673/ N507673
T-DNA mutant line of <i>A. thaliana</i> (insertion in At1g19250) (<i>fmo1</i>)	NASC; Mishina and Zeier, 2006	SALK_026163/ N526163
EMS (ethyl methanesulfonate) mutant line of <i>A. thaliana</i> (At1g74710) (<i>sid2-1</i>)	Nawrath and Métraux, 1999	Tair Accession - Polymorphism:1948014
EMS (ethyl methanesulfonate) mutant line of <i>A. thaliana</i> (At1g64280) (<i>npr1-2</i>)	NASC	N3801
EMS (ethyl methanesulfonate) mutant line of <i>A. thaliana</i> (At3g52430) (<i>pad4-1</i>)	NASC	N3806
T-DNA mutant line of <i>A. thaliana</i> (insertion in At5g52810) (<i>sard4-5</i>)	NASC; Hartmann et al., 2017	N441041 (GK-428E01)
EMS (ethyl methanesulfonate) mutant line of <i>A. thaliana</i> (At3g48090) (<i>eds1-2</i>)	Bartsch et al., 2006	Tair Accession Polymorphism:1009135505

(Continued on next page)

Continued		
REAGENT or RESOURCE	SOURCE	IDENTIFIER
Oligonucleotides		
FMO1-F1 (oligos for sticky end cloning into pET32b): TATGGCTTCTAACTATGATAAGCTTACTTC	This paper	N/A
FMO1-F2 (oligos for sticky end cloning into pET32b): TGGCTTCTAACTATGATAAGCTTACTTC	This paper	N/A
FMO1-R1 (oligos for sticky end cloning into pET32b): GAGCAGTCATATCTCTTTTCTTCTTG	This paper	N/A
FMO1-R2 (oligos for sticky end cloning into pET32b): TCGAGAGCAGTCATATCTCTTTTCTT	This paper	N/A
Software and Algorithms		
Fiji (image processing package based on ImageJ)	NIH	https://fiji.sc/#
CLC Genomics Workbench	QIAGEN	https://www.qiagenbioinformatics.com/products/clc-genomics-workbench/
edgeR (Bioconductor)	Bioconductor	https://bioconductor.org/packages/release/bioc/html/edgeR.html
MapMan	Hosted at Forschungszentrum Juelich, Germany	http://mapman.gabipd.org/de/mapman-download
R statistical package (R version 3.4.2)	The R Foundation	https://www.r-project.org/
Essential FTIR software v3.10.037	Operant LLC	http://www.essentialftir.com/
Zeiss Zen 2 core imaging software	Carl Zeiss Microscopy GmbH	https://www.zeiss.de/mikroskopie/produkte/mikroskopsoftware/zen-2-core.html
Phylogenetic Analysis (Phylogeny.fr)	Laboratoire Information Génomique et Structurale (IGS), CNRS (France)	http://www.phylogeny.fr/phylogeny.cgi
BlastP	NCBI	https://blast.ncbi.nlm.nih.gov/Blast.cgi?PAGE=Proteins
Other		
Volatile collection trap - VCT-1-/4-3-Por-Q (Porapak-Q absorbent)	Volatile Collection Trap (VCT) LLC	http://www.volatilecollectiontrap.com/main.sc

CONTACT FOR REAGENT AND RESOURCE SHARING

Further information and requests for resources and reagents should be directed to and will be fulfilled by the Lead Contact, Jürgen Zeier (juergen.zeier@hhu.de).

EXPERIMENTAL MODEL AND SUBJECT DETAILS

Arabidopsis

Arabidopsis thaliana plants were grown individually in pots containing a mixture of soil (Substrat BP3; Klasmann-Deilmann), vermiculite, and sand (8:1:1) in an environmentally controlled cultivation chamber with a 10-h-day (9 AM to 7 PM)/14-h-night cycle. Relative humidity in the growth chambers was adjusted to 60% and day and night temperatures were set to 21°C and 18°C, respectively. For inoculation experiments with *Pseudomonas syringae* (metabolite and isotope-labeling studies, assessment of basal resistance), 5- to 6-week-old plants with an unstressed, uniform appearance were used, whereas experiments with *Hyaloperonospora arabidopsidis* were performed with 3- to 4-week-old, naive plants, if not stated otherwise. The *ald1* and *fmo1* mutants represent the SALK lines SALK_007673 and SALK_026163, respectively (Mishina and Zeier, 2006; Návarová et al., 2012). Further *sid2-1* (*sid2*, *ics1*), *npr1-2* (*npr1*); NASC ID: N3801), *pad4-1* (*pad4*), *sard4-5* (*sard4*; GABI_428E01) and *eds1-2* (*eds1*; Bartsch et al., 2006) were used in this study (see Bernsdorff et al., 2016 and Hartmann et al., 2017 for a more detailed description). All *Arabidopsis* mutant lines used are in the Col-0 background.

Pseudomonas

Pseudomonas syringae pv. *maculicola* ES4326 (*Psm*) and *Psm* carrying the *Photobacterium luminescens luxCDABE* operon (*Psm lux*) were grown at 28°C in King's B medium containing the appropriate antibiotics (concentrations: rifampicin 50 µg L⁻¹, kanamycin 50 µg L⁻¹, tetracycline 15 µg L⁻¹) under permanent shaking (Zeier et al., 2004; Fan et al., 2008). For experiments, overnight log-phase cultures were washed four times with 10 mM MgCl₂ solution and diluted to different final OD₆₀₀ levels for leaf inoculation as detailed in

the respective sections. In general, the diluted bacterial solutions as well as mixtures thereof containing metabolites of interest, such as labeled isotopes, were carefully pressure infiltrated from the abaxial side of the leaves using a needleless syringe.

Hyaloperonospora arabidopsidis (Downy Mildew)

The oomycete *Hyaloperonospora arabidopsidis* (*Hpa*) is the causal agent of downy mildew in the model plant *Arabidopsis* and has been extensively studied in the context of host/pathogen co-evolution (Holub et al., 1994). Due to its obligate biotrophic life cycle, *Hpa* has to be maintained on a weekly basis on susceptible *Arabidopsis* accessions and mutants to ensure its survival. In our study, *Arabidopsis* Col-0 wild-type plants were used for the propagation of the compatible *Hpa* isolate Noco2 (Bartsch et al., 2006). Therefore, 2 week old *Arabidopsis* plants (50-100 individuals/pot) were spray-inoculated with a suspension of 5×10^4 sporangia per ml of water until the leaves were saturated. The inoculated plants were then maintained on sealed trays with a transparent lid under short day (10 hours light period/18°C during day and night) and high humidity conditions (> 90% humidity) in an environmentally controlled growth chamber (Percival Scientific: Model SE-41).

METHOD DETAILS

GC-MS analysis of metabolites

In this study, two major analytical procedures for plant metabolite extraction and derivatization were used. The first method converts free carboxylic acids into the respective methyl esters after sample derivatization with trimethylsilyl-diazomethane. This optimizes GC separation of organic acids (Hartmann et al., 2017). This procedure was mainly used for the initial identification of NHP from plant tissues and analysis of enzyme assays. The second method is based on the trimethylsilylation of carboxyl-, hydroxyl- and amino-groups of the sample analytes and was employed for the quantification of NHP and other target metabolites in plant tissue and as an alternative procedure for the identification of NHP.

The first method has been described in detail previously (Návarová et al., 2012; Hartmann et al., 2017). Levels of NHP and other metabolites in *Arabidopsis* leaf samples or from enzyme activity assays were determined after solvent extraction of the samples material followed by a vapor-phase extraction-based work up of the extracts and subsequent analysis of the resulting derivatized samples. Shock-frozen leaf material (approximately 100-200 mg pooled from up to six leaves) was ground to a fine powder using a pre-chilled ball mill and immediately homogenized with 600 μ l of extraction buffer, consisting of H₂O:1-propanol:HCl (1:2:0.005). In the case of enzyme assays, 50-100 μ l of the aqueous assays were used and extracted as described above. After the addition of 100 ng of D₄-salicylic acid as internal standard, 1 mL of methylene chloride was added and the mixture was thoroughly re-homogenized (> 30 s) and then centrifuged at 14000 x g for 1 min to achieve optimal phase separation. For the analyses of NHP, the lower organic phase was removed, dried with Na₂SO₄, and incubated with 4 μ l of 2 M trimethylsilyl-diazomethane in hexane (Sigma-Aldrich) for 5 min at room temperature, driving the conversion of carboxylic acids into the corresponding methyl esters. The methylation reaction was stopped by addition of an excess of acetic acid (4 μ l of a 2 M solution in hexane) to the vials, and the sample was then subjected to a vapor phase extraction procedure at 70°C and 200°C under a steady stream of nitrogen by using a volatile collector trap packed with Porapak-Q absorbent (VCT-1/4X3-POR-Q; Analytical Research Systems). The volatilized and trapped metabolites were then eluted from the absorbent with 1 mL methylene chloride. Finally, the sample volume was reduced to 30 μ l in a stream of nitrogen prior to GC-MS analysis. 4 μ l of the resulting sample mixture were then separated on a gas chromatograph (GC 7890A; Agilent Technologies) equipped with a fused silica capillary column (ZB5-MS, Zebron) and mass spectra were recorded with a 5975C mass spectrometric detector (Agilent Technologies) in the electron ionization (EI) mode as described before (Návarová et al., 2012; Hartmann et al., 2017). GC-MS data was evaluated using MSD ChemStation software version E.02.01.1177 (Agilent Technologies). NHP was analyzed by the selected ion chromatogram of mass-to-charge ratio (m/z) 100.

For the second method, 40-60 mg of freshly pulverized, frozen leaf tissue were extracted twice with 1 mL of MeOH/H₂O (80:20, v/v) extraction buffer. The buffer for the initial extraction step was additionally supplemented with various internal standards, including D₉-Pip (1000 ng) for the quantification of Pip, D₄-SA (500 ng) for the quantification of SA and 2-hydroxy-cyclohexanecarboxylic acid (2-HCC; 1000 ng) for the quantification of NHP. During each individual extraction step, samples were first homogenized thoroughly by vortexing (> 30 s) and then incubated on a rotary mixer (150 rpm/min) at 4°C for at least 5 min. Afterward samples were centrifuged for 2 min at 14000 x g and the supernatants from both extraction steps (2 mL total volume) combined into one 2 mL Eppendorf vial. At this stage, samples could be stored for several days at -80°C. For subsequent derivatization, aliquots of 400 to 800 μ L of this extract were evaporated to dryness using a ScanSpeed vacuum centrifuge (Labogene ApS, Denmark). The derivatization procedure itself started with the addition of 20 μ l pyridine, followed by 20 μ l N-methyl-N-trimethylsilyltrifluoroacetamide (MSTFA) containing 1% trimethylchlorosilane (v/v) and 60 μ l of hexane. Between each pipetting step, the sample vials were thoroughly vortexed. The resulting reaction mixture was first incubated for 30 min at 70°C and then allowed to cool down at room temperature for an additional 30 min. Finally, aliquots of the samples were transferred to a GC vial and diluted 5- to 10-fold with hexane. 2 μ l of the sample mixture were then separated on a gas chromatograph (GC 7890A; Agilent Technologies) equipped with a fused silica capillary column (Phenomenex ZB-35; 30 m x 0.25mm x 0.25 μ m) and mass spectra were recorded with a 5975C mass spectrometric detector (Agilent Technologies) in the electron ionization (EI) mode. The GC oven temperature program was as follows: initial temperature of 70°C for 2 min, followed by a gradient to 320°C at a rate of 10°C/min, followed by a final hold time of 5 min (Total run time: 32 min). For quantitative determination of individual metabolites, peaks originating from selected chromatograms of a

specific m/z ratio were integrated and quantified by relating the areas of a substance peak to the peak area of the corresponding internal standard (IS) using MSD ChemStation software version E.02.01.1177 (Agilent Technologies): NHP (m/z 172) / IS: 2-HCC (m/z 273); Pip (m/z 156) / IS: D₉-Pip (m/z 165); SA (m/z 267) / IS: D₄-SA (m/z 271). Correction factors experimentally determined for each substance by use of authentic substances were considered. Metabolite levels were related to leaf fresh weight.

For the quantification of metabolites, at least six plants per treatment and plant genotype were analyzed, whereby individual replicate leaf samples ($n \geq 3$) were pooled from two plants. The experiments depicted in the figures were repeated several times with similar results.

GC-FTIR analysis of metabolites

GC-IRD spectra were acquired as detailed in [Hartmann et al. \(2017\)](#). Briefly, spectra were recorded with a resolution of 16 cm^{-1} and a scan rate of eight scans per second using a Hewlett-Packard 6890 Series gas chromatograph coupled with an IRD3 infrared detector manufactured by ASAP analytical (Analytical Solutions and Providers, Covington, KY – USA). The IRD method parameters were as follows: Resolution = 16; Apodization = Triangle; Phase correction = Mertz; Zero-Fill = 1; Co-Add = 2. Flow cell and the transfer line temperatures were both set to 250°C . Nitrogen was used as flow cell sweep gas. The GC was operated in splitless mode using helium as carrier gas, with a flow rate adjusted to 2 ml/min and a column head pressure of 9.54 psi. The GC-IRD studies were carried out with a fused silica capillary column (Zebron ZB-5; 30 m x 0.32 mm x 0.25 μm) purchased from Phenomenex Corporation (Aschaffenburg, Germany). The GC oven temperature program was as follows: an initial temperature of 50°C for 3 min, ramped up to 240°C for 8 min, followed by a ramping step to 320°C over the course of 20 min (Total time: 33.75 min). In general, 1–4 μl of a respective, derivatized sample were injected using an Agilent 7863 Series autoinjector. To simplify the identification of relevant target peaks, all method parameters including the derivatization of the samples by trimethylsilyl-diazomethane (yielding methylesters of carboxylic acids), the GC column, as well as the temperature program used in our GC-IRD studies were identical to those used in the complementing GC-MS studies. For the analysis of FTIR data, Essential FTIR software v3.10.037 was used (Operant LLC; Madison WI - USA).

Chemical synthesis of N-hydroxypipicolinic acid

Authentic 1-hydroxypiperidine-2-carboxylic acid (N-hydroxypipicolinic acid, NHP) was synthesized according to a protocol of [Murahashi and Shiota \(1987\)](#). 0.232 g of Na_2WO_4 (0.70 mmol) were dissolved in 12 mL of water. To this solution, an amount of 1.5 g of piperidine (17.62 mmol) was added and the solution cooled down to 0°C . An aqueous 30% solution of H_2O_2 in water was added slowly (4.02 ml, 39.55 mmol H_2O_2). The resulting solution was stirred for further 3 h at 0°C . Then, 1.72 g of potassium cyanide (26.41 mmol) was added to the solution, followed by the careful addition of 6.3 mL 4 N aqueous HCl. The reaction mixture was stirred for 4 h at $0\text{--}10^\circ\text{C}$. Afterward, the solution was adjusted to pH 9 with 2 N of aqueous KOH solution. The product was extracted with dichloromethane and the solvent was evaporated under reduced pressure. 1.47 g of 1-hydroxypiperidine-2-carbonitrile (11.65 mmol, 66 %) were isolated. 1 g (7.93 mmol) of this product was dissolved in 13 mL concentrated HCl and heated until reflux for 18 h. Removal of the solvent under reduced pressure yielded 1.76 g (7.49 mmol, 94%) 1-hydroxypiperidine-2-carboxylic acid hydrochloride with nearly equimolar amounts of ammonium chloride (^1H - and ^{13}C -NMR spectral data, mass spectrum and elemental composition provided in [Figure S3G](#)).

Plant treatments with Pip and NHP

Treatments with Pip and NHP were performed with the established procedure described in [Návarová et al. \(2012\)](#). With respect to *P. syringae* resistance assays, 10 mL of a 1 mM aqueous solution of Pip or NHP (equates to 10 μmol) were pipetted onto the soil of individually cultivated 5-week-old plants. The same exogenous application of 10 mL H_2O served as a control treatment. With respect to *Hpa* resistance assays, 3 to 4-week old plants were cultivated in batches of four plants per pot and treated as described in “Assessment of plant resistance to *Hpa*.” Inoculation with *P. syringae* or *Hpa* was performed 24 h after the plant pre-treatment as described below (“Assessment of plant resistance to *P. syringae*”).

Assessment of plant resistance to *P. syringae*

To assess bacterial growth in naive 5-week-old plants, overnight log phase cultures of *Psm lux* were washed three times with 10 mM MgCl_2 and diluted to a final optical density at 600nm (OD_{600}) = 0.001 before infiltrating the resulting bacterial suspensions from the abaxial side into three fully grown leaves of either untreated or pre-treated *Arabidopsis* plants (compare section: Plant treatments with Pip and NHP) using a 1 mL syringe without a needle. The infiltration was performed between 10 and 11 AM. Approximately 60 hours later, the bacterial growth was quantified by measuring the bacterial bioluminescence in leaf discs (10 mm in diameter) of infiltrated leaves (one disc per leaf, three discs per plant) using a Sirius FB12 luminometer (Berthold Detection Systems). Bacterial growth rates were displayed as relative light units per cm^2 of leaf area ([Fan et al., 2008](#)). For each independent experiment, at least 20 replicate leaves ($n \geq 20$) from six to seven plants per treatment and plant genotype were measured before performing a statistical analysis of the resulting values. All pathogen experiments depicted in the figures were repeated several times with similar results.

Assessment of plant resistance to *Hpa*

2-, 3-, or 4-week old plants were spray-inoculated with a suspension of sporangia ($5 \times 10^4 \text{ ml}^{-1}$) of the *Hpa* isolate Noco2 as described in the section “*Hyaloperonospora arabidopsidis* (Downy Mildew).” 7 days after inoculation, leaves of plants were photographed to

document the presence/absence of disease symptoms and then harvested and stained with Trypan-blue for further microscopic analysis. At least 10 replicate leaves ($n \geq 10$) from five plants per treatment and plant genotype were examined and the resulting values statistically analyzed. Independent experiments were conducted three times with similar results.

Trypan Blue Staining

Trypan blue staining was performed to enable the identification and quantitative analysis of disease stages and resistance phenotypes after *Hpa* infection (Uknes et al., 1992; Bartsch et al., 2006). Briefly, leaves of *Hpa*-inoculated plants were harvested in 50 mL conical tubes (Falcon) and covered with trypan blue solution, more specifically lactic acid–phenol–trypan blue solution, consisting of 1 mg/ml trypan blue, 25 % [w/v] lactic acid, 25 % water-saturated phenol [v/v], and 25 % glycerol [v/v] in water. The fully submerged samples were incubated overnight at 37°C under permanent shaking (200 rpm). The trypan blue solution was replaced the next day by a 2.5 g/ml chloral hydrate aqueous solution and incubated under the same conditions until the leaves were decolorized. Finally, the chloral hydrate was replaced with 50% glycerol for further storage or mounting of the samples on microscope slides prior to their examination under a light microscope equipped with interference or phase-contrast optics.

Microscopic analysis of *Hpa* infection

Microscopic photographs of Trypan blue-stained leaves were acquired with a Zeiss AxioCam 105 color camera coupled to a bright field microscope (Zeiss AxioStar Plus, Carl Zeiss Ltd.) operated by Zeiss ZenCore software. In addition, leaf overview images were captured with a Canon EOS 6D DSLR camera equipped with a Canon MP-E 65mm Macro f/2.8 manual focus lens and a light table adjusted to daylight conditions (5500 Kelvin) as light source (compare Figure 6B). Leaf images were subsequently analyzed using the ImageJ-based analysis software bundle Fiji (Schindelin et al., 2012). Leaf surface areas, the lengths of free intercellular hyphae (IH; Figure 6B, image I), and the lengths of intercellular hyphae encased by trailing necrotic cells (TN; Figure 6B, image IV) were determined in overview shots with the freehand line selection tool and the measuring function of Fiji. Beforehand, the length scale was set in Fiji using photographs of a calibrated benchmark taken under the same photographic and microscope settings as the leaf images. Total IH were calculated as the sum of free IH and IH encased in TN. The number of oospores (OS; Figure 6B, image III) were determined in leaf photographs with the multi point tool of Fiji. The number of sporangiophores (SP; Figure 6B, image II) on the leaf samples was assessed by direct microscopic examination of sample slides and counting of SP with the help of marked 1 mm-grids. In order to minimize the variation of measurements, the parallel leaf samples were examined and photographed with the same microscope settings. To reduce user-generated bias, the images were additionally randomized and analyzed independently.

Treatment with Isotope-Labeled Metabolites

In planta labeling experiments were performed by infiltrating three to four mature leaves of 5-week-old soil-grown *Arabidopsis* wild-type Col-0 and relevant mutant plants in the morning with *Psm* ($OD_{600} = 0.005$) or $MgCl_2$ (mock controls) as described before (Section: Assessment of Plant Resistance to *P. syringae*). Four hours after the initial inoculation, the same leaves were infiltrated with 5 mM solutions of the isotope-labeled L-Lys varieties L-Lys-6- ^{13}C - ϵ - ^{15}N and L-Lys-4,4,5,5- d_4 (d_4 -Lys) (Sigma-Aldrich) prepared in HPLC-grade water. DL-2-piperidine- d_9 carboxylic acid (D_9 -Pip; Aldrich 688444) was co-infiltrated at a final concentration of 1 mM as part of the final bacterial suspension. In all cases, water infiltrations served as control treatments. Infiltrated leaves were harvested at 48 hpi (counting from the first infiltration event with *Psm* or mock treatment) and subsequently extracted, derivatized, and analyzed by GC-MS according to the described protocols.

Cloning of FMO1

cDNA fragments corresponding to FMO1 (At1g19250) were PCR-amplified using high-fidelity Phusion polymerase (New England Biolabs) as recommended by the manufacturer. The cDNA sequence of FMO1 (NCBI Reference Sequence accession number: NM_101783.4) was introduced into the target vector pET32b(+) (Novagen) using sticky-end cloning between restriction sites *Nde*I and *Xho*I. The resulting recombinant protein thus contained eight non-native residues at the C terminus, including the poly-Histidine tag. Primer sequences can be found in the Key resources table. Plasmids harboring the respective genes were transformed into chemically competent *E. coli* BL21 Rosetta 2(DE3) pLysS cells (Novagen) and plated on LB-Agar plates containing the appropriate selection markers. Positive transformants carrying the gene of interest were identified by colony PCR using the same gene-specific primers used for the initial amplification and were verified by sequencing.

Purification of recombinant FMO1 enzyme

A single colony of recombinant *E. coli* BL21 Rosetta 2(DE3) pLysS cells containing FMO1 inserted into pET32b vector was picked and cultured overnight in 3 mL of lysogeny broth (LB) medium supplemented with the appropriate selection markers at 37°C and with constant shaking on an orbital shaker before inoculating and growing a 500-1000 mL culture under the same conditions until the OD_{600} reached 0.5-0.8. At this point the culture was briefly cooled down and the transgene expression was induced with 0.5 mM isopropyl- β -D-1-thiogalactopyranoside (IPTG), followed by incubation overnight at 16°-25°C with constant shaking (240 rpm). Generally, the best results were obtained with freshly transformed cells and incubation at reduced temperatures (16°C) after induction of transgene expression to minimize the precipitation of recombinant enzymes as insoluble inclusion bodies. Satisfying results were also obtained with shorter incubation times (5 h at 28°C after induction with IPTG), even though it should be mentioned that we

initially also met severe solubility problems as reported for other N-hydroxylating flavoprotein monooxygenases in the past (summarized by [Olucha and Lamb, 2011](#)). The bacterial pellets were collected by centrifugation at 3220 x g for 15 min at 4°C (Eppendorf 5810R). The pellet was then re-suspended in a minimum of extraction/binding buffer (50 mM sodium phosphate, pH 8.0, 500 mM NaCl, 10% glycerol, 20 mM imidazole, 5 mM β -mercaptoethanol, 1 mM PMSF). For bigger culture volumes (> 500 ml), the resulting homogenate was transferred to a pre-cooled mortar and ground in liquid nitrogen with a pestle until a homogeneous white powder was obtained. The powder was then transferred to 2 mL Eppendorf tubes and allowed to thaw on ice. The resulting homogenate was then precipitated using a centrifuge at 20000 x g for 30 min at 4°C (Eppendorf 5417C). The cell-free supernatants containing soluble recombinant protein were collected, pooled and filtered through a low-protein binding nylon filter (0.22 μ m) before being applied to a pre-equilibrated immobilized immune affinity chromatography (IMAC) column, such as a nickel-charged His GraviTrap affinity column (GE Healthcare, Germany) or cobalt-charged HisTALON Gravity column (Takara Bio, USA) (1 ml). After the initial binding step, the column was successively washed according to the respective manufacturers recommendations. The proteins were then eluted with 50 mM sodium phosphate buffer, pH 8.0, containing up to 500 mM NaCl and 200 mM imidazole and collected in fractions of 0.75 ml. Using those conditions, most of the enzyme activity was found to be in 4-5 consecutive fractions, which were combined and desalted using a 5 mL desalting PD10 column (GE Healthcare) equilibrated with a low-salt buffer, containing 100 mM potassium phosphate buffer (pH 8), containing 10% (v/v) glycerol and 1 mM DTT. Aliquots of the purified proteins were used for the quantification of total protein content by the Bradford method using the Bradford Assay reagent (Bio-Rad, Düsseldorf, Germany) according to the manufacturer's protocol. Bovine serum albumin (Albumine fraction V) was used for the standard curve. Target enzyme purity was determined by SDS-polyacrylamide gel electrophoresis on a 12% gel according to Laemmli's method. Due to the relative instability of the purified recombinant protein (loss of 90% of its activity within 24 h of the purification), the majority of the enzymes was used directly for activity assays and the remaining protein was flash frozen in liquid nitrogen and stored at -80°C in 20% glycerol for later analysis.

FMO1 activity assays

FMO1 enzyme assays were designed based on the knowledge about mechanistic and structural studies of the few characterized N-hydroxylating flavoprotein monooxygenases ([Olucha and Lamb, 2011](#)). In general, standard assays were carried out with 50 mM sodium phosphate buffer, pH 8.0, containing 50 μ g ml⁻¹ recombinant FMO1 protein, 400 μ M NADH, 10 mM L-pipecolic acid, and 200 μ M flavin adenine dinucleotide (FAD⁺) at 30°C. All reaction mixtures contained 5% glycerol for additional enzyme stability and were incubated for up to 16 h. Reactions were stopped by inactivating the enzyme at 85°C for 10 min. The formation of NHP was monitored using GC-MS after derivatization of the assays with the methylating reagent trimethylsilyl-diazomethane as described above. Reactions without enzyme or heat-inactivated FMO1 enzyme were systematically performed as controls. All assays were repeated at least in triplicates.

Genome-Wide Analyses of the Plant Transcriptional Response to Pip

To examine the transcriptional response of *Arabidopsis* Col-0 and *fmo1* to elevated Pip, individual, 5-week-old plants were supplied with 10 μ M Pip or control-treated with water as described above (Plant treatments with Pip and NHP; [Návarová et al., 2012](#)). Three biologically independent, replicate experiments were performed. In each experiment, at least 4 full-grown leaves from 6 different plants were harvested one day after the treatment and pooled for one biological replicate. In this way, 3 biologically independent, replicate samples per treatment and plant genotype were obtained. RNA-seq analysis of the resulting 12 samples was performed according to [Bernsdorff et al. \(2016\)](#) with minor modifications. RNA of leaf samples was extracted with the Plant RNeasy extraction kit (QIAGEN, Germany), and treated on-column (QIAGEN, Germany) and in solution with RNA-free DNase (New England Biolabs, MA, USA). The integrity of RNA, quality of the sequencing library and fragment sizes was checked on a 2100 Bioanalyzer (Agilent, CA, USA). Libraries were prepared using the TruSeq RNA Sample Prep Kit v2 (Illumina, San Diego, CA) and library quantification was performed with a Qubit 2.0 (Invitrogen, Germany). Leaf samples were multiplexed 12 libraries per lane, yielding approximately 150 million reads per lane. All libraries were sequenced on the HISEQ2500 Illumina platform (San Diego, CA). Libraries for the not stranded RNA-seq experiments were sequenced in the single end (SE) mode with length of 50 or 100 nucleotides.

De-multiplexing and mapping of reads to the *Arabidopsis thaliana* genome was performed by CLC bio Genomics Workbench© with default parameters (alignment over at least 80 % of the length of the read, up to three mismatches allowed) without alternative transcript detection. Differential expression between Pip- and water-treated samples was calculated as a pairwise using likelihood ratio test on raw read counts as described in the edgeR user's guide (www.bioconductor.org; see section Statistical Analyses). Genes were considered significantly differentially expressed with an FDR below 0.05 ([Benjamini and Hochberg, 1995](#)). Reads per million (rpm) are reported for all transcripts. Rpm were averaged for the replicates of each condition and the log₂ of fold-changes between Pip- and water values (= P/H-fold changes; [Figure S2](#)) were calculated by formally adding one read to all rpm values to account for transcripts with no expression detected in one or more samples before fold-change calculation and logarithmic transformation. This allowed keeping genes with very low basal expression values but marked Pip-induced expression in the datasets without significantly changing the actual logarithmized P/H-ratios. The complete RNA-seq data of the Pip-response experiments are provided in [Table S1](#). The comparative RNA-seq data for the biological SAR response in the wild-type represent the Col-0 data of the "SAR experimental data set II" of [Bernsdorff et al. \(2016\)](#) and also consists of 3 biological replicates for both *Psm*- and mock-treated samples. The SAR data was evaluated in the same manner than the Pip response data ([Table S2](#)). The *Arabidopsis*

transcripts were annotated with descriptions from TAIR10 and functional annotations from MapMan. To determine the proportions of Pip⁺ and SAR⁺ genes in gene families (<http://www.arabidopsis.org/>), MapMan categories, and hormone-inducible genes, the respective gene sets were aligned to the RNA-seq datasets using Microsoft Excel.

Phylogenetic analysis of potential FMO1 orthologs

BLAST searches were carried out with an E-value of 10^{-5} and required proteins to align along at least 50% of their length. After selection of a core dataset of protein sequences with a special focus on plant species with either commercial or nutritional value (30 sequences), the phylogenetic analysis was performed using the Phylomeny.fr analysis pipeline (<http://www.phylomeny.fr/phylogeny.cgi>) (Dereeper et al., 2008).

QUANTIFICATION AND STATISTICAL ANALYSIS

The procedures for the detailed quantification of gene expression, metabolites, as well as disease and resistance parameters are described in the respective [Method Details](#) subsections. The results presented in this study are generally derived from one experimental dataset, consisting of at least three biological replicates per treatment and genotype for metabolite analyses ($n \geq 3$), a minimum of twenty leaf replicates for *P. syringae* growth assays ($n \geq 20$), and a minimum of ten leaf replicates for the assessment of *Hpa* infection structures and resistance parameters ($n \geq 10$). The represented results were confirmed in at least three independent experiments. ANOVA analyses with type II sum of squares were performed on \log_{10} -transformed values to assess statistical differences of datasets. Therefore, the R statistical package (<https://www.r-project.org/>) with the command “aov(Phenotype; Treatment + Genotype + Treatment * Genotype, data=object1)” (with object1 being the data table loaded into the R workspace) was used, and subsequent posthoc Tukey’s HSD test was performed (Bemsdorff et al., 2016). Pairwise comparisons of treatment versus control values were performed with a two-tailed Student’s t test in Microsoft Excel.

To test for differential expression of the 28496 genes covered by the RNA-seq analyses, a likelihood ratio test on raw read counts of the three replicate treatment and control values was performed as described in the edgeR user’s guide (www.bioconductor.org). Therefore, the R statistical package was used with the following sequence of commands:

```
> library(edgeR)
> x <- read.delim("datainputfile.txt", row.names = "Name")
> group <- factor(c(1,1,1,2,2,2))
> y <- DGEList(counts = x, group = group)
> y <- calcNormFactors(y)
> design <- model.matrix(~group)
> y <- estimateDisp(y, design)
> fit <- glmFit(y, design)
> lrt <- glmLRT(fit, coef = 2)
> options(max.print = 99999999)
> sink("output.txt")
> topTags(lrt, n = 28496, adjust.method = "BH," sort.by = "none," p.value = 1)
```

To determine whether gene categories were significantly enriched or depleted in Pip⁺ and SAR⁺ genes, Fisher’s exact test corrected according to [Benjamini and Hochberg \(1995\)](#) was used.

DATA AND SOFTWARE AVAILABILITY

The accession numbers for the RNA-seq data reported in this paper are ArrayExpress: E-MTAB-6243 (Pip response) and E-MTAB-4151 (SAR; Col-0 data from experimental set 2).

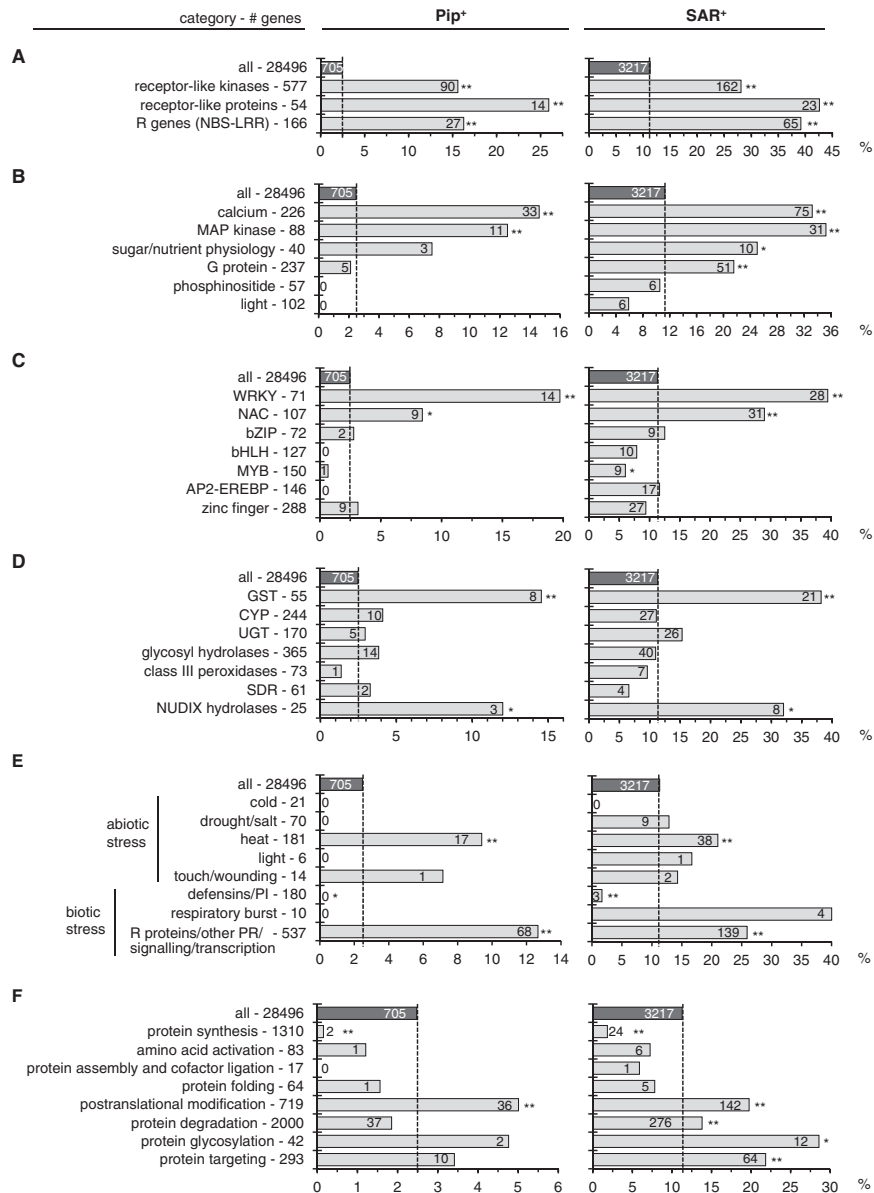


Figure S1. Proportions of Pip⁺ and SAR⁺ Genes in Defined Gene Groups Representing MapMan Functional Categories and Arabidopsis Gene Families, Related to Figure 1 and Tables S1 and S2

Dashed vertical lines illustrate the percentage of Pip⁺ and SAR⁺ genes in the whole, RNA-seq-covered transcriptome (28496 genes). The total number (#) of genes in each category is indicated on the left. The absolute number of Pip⁺ and SAR⁺ genes within a particular gene category is indicated on the respective horizontal bar. Asterisks next to the bars indicate significant enrichment (or depletion) of gene categories in Pip⁺ or SAR⁺ genes (**: p < 0.001; *: p < 0.05; Fisher's exact test). Please note the large congruence between the transcriptional response to elevated Pip (Pip⁺ genes) and the biologically induced SAR response (SAR⁺ genes). (A) Gene families involved in elicitor perception. Genes coding for nucleotide binding site (NBS)-containing resistance (R) proteins, receptor-like protein kinases and receptor-like proteins were strongly enriched within the Pip⁺ genes, indicating that Pip positively regulates the expression of genes involved in pathogen perception.

(B) Genes and gene families involved in (defense) signal transduction. Genes associated with calcium signaling and mitogen-activated protein kinase (MPK) signal transductions were significantly overrepresented in the Pip⁺ group.

(C) Main transcription factor families. Specifically, genes of the WRKY and NAC transcription factor families were significantly overrepresented within the Pip⁺ genes.

(D) Genes of different enzyme classes (GST: glutathione-S-transferases; CYP: cytochrome P450 superfamily; UGT: UDP-dependent glycosyltransferases; SDR: short chain dehydrogenases). Significant enrichments of glutathione-S-transferase and NUDIX hydrolase genes were discernible in the Pip⁺ group.

(E) MapMan functional category "stress" with subcategories belonging to the groups "biotic stress" and "abiotic stress." In the category "biotic stress," the terms "R proteins / other PR / signaling / transcription" were strongly enriched in the Pip⁺ gene group, whereas the terms "respiratory burst" or "defensins/

(legend continued on next page)

proteinase inhibitors” were not represented. Elevated Pip also induced a significant number of genes of the “abiotic stress” subcategory “heat,” whereas genes from the bins “cold” or “drought/salt” were not induced.

(F) Subcategories of the MapMan functional category “protein.” An enrichment of the gene classes “posttranslational modification” was evident in the Pip⁺ gene group, whereas genes from the class “protein synthesis” were strongly underrepresented.

AGI Code	Name	Pos.	Gene Name / Description	Mean Expression Value				Fold-change (log ₂)		SAR ⁺ gene
				Col-0 H ₂ O	Col-0 Pip	<i>fmo1</i> H ₂ O	<i>fmo1</i> Pip	Col-0 P/H	<i>fmo1</i> P/H	
A At3g11340	UGT76B1	5	UDP-DEPENDENT GLYCOSYLTRANSFERASE 76B1	0.4	24.0	0.0	0.1	4.2**	0.0	+
At3g26830	<i>PAD3</i>	19	PHYTOALEXIN DEFICIENT 3	1.4	33.8	0.4	1.0	3.9**	0.5	+
At2g13810	<i>ALD1</i>	24	AGD2-LIKE DEFENSE RESPONSE PROTEIN 1	0.3	17.7	0.0	0.1	3.8**	0.2	+
At2g14610	<i>PR1</i>	48	PATHOGENESIS-RELATED GENE 1	0.6	16.8	0.1	1.2	3.5**	1.0	+
At3g25882	<i>NIMIN-2</i>	50	NIM1-INTERACTING 2	1.2	23.1	0.5	0.8	3.5**	0.3	+
At5g13320	<i>PBS3</i>	51	AVRPPHB SUSCEPTIBLE 3	7.4	90.0	5.2	7.4	3.4**	0.4	+
At1g73805	<i>SARD1</i>	62	SAR DEFICIENT 1	7.1	80.0	2.2	3.0	3.3**	0.3	+
At4g39030	<i>EDS5</i>	67	ENHANCED DISEASE SUSCEPTIBILITY 5	3.7	44.1	2.2	3.2	3.3**	0.4	+
At1g19250	<i>FMO1</i>	107	FLAVIN-DEPENDENT MONOOXYGENASE 1	0.3	8.3	0.0	0.0	2.9**	0.0	+
At5g10760	<i>AED1</i>	123	APOPLASTIC, EDS1-DEPENDENT 1	12.2	92.3	5.3	9.0	2.8**	0.7	+
At3g12580	<i>HSP70</i>	126	HEAT SHOCK PROTEIN 70	6.2	48.2	8.4	7.2	2.8**	-0.2	+
At1g74710	<i>ICS1</i>	139	ISOCHORISMATE SYNTHASE 1	19.5	131.4	13.9	14.2	2.7**	0.0	+
At3g52430	<i>PAD4</i>	164	PHYTOALEXIN DEFICIENT 4	17.0	106.1	13.4	14.3	2.6**	0.1	+
At1g02450	<i>NIMIN1</i>	176	NIM1-INTERACTING 1	0.3	6.2	0.0	0.0	2.5*	0.0	+
At5g24530	<i>DMR6</i>	192	DOWNY MILDEW RESISTANT 6	40.2	220.9	10.1	20.3	2.4**	0.9	+
At4g12720	<i>NUDT7</i>	218	NUDIX HYDROLASE HOMOLOG 7	27.8	143.6	23.3	27.0	2.3**	0.2	+
At5g52810	<i>SARD4</i>	221	SAR DEFICIENT 4	17.7	91.9	12.9	13.1	2.3**	0.0	+
At5g26920	<i>CBP60G</i>	236	CALM-BINDING PROTEIN 60-LIKE G	15.1	76.8	10.9	9.6	2.3**	-0.2	+
At4g14400	<i>ACD6</i>	247	ACCELERATED CELL DEATH 6	376.7	1752.9	77.4	161.1	2.2*	1.0	+
At3g09830	<i>PCRK1</i>	264	PTI COMPROMISED RECEPTOR-LIKE CYTOPLASMIC KINASE 1	10.1	48.9	8.6	9.5	2.2**	0.1	+
At1g59870	<i>PEN3</i>	265	PENETRATION 3	210.7	951.1	179.3	202.9	2.2**	0.2	+
At3g48090	<i>EDS1</i>	305	ENHANCED DISEASE SUSCEPTIBILITY 1	22.7	96.6	14.2	18.8	2.0**	0.4	+
At1g75040	<i>PR5</i>	344	PATHOGENESIS-RELATED GENE 5	35.5	137.6	16.5	18.6	1.9**	0.2	+
At1g65690	<i>NHL6</i>	353	NDR1/HIN1-LIKE 6	0.7	5.4	0.3	0.6	1.9*	0.3	+
At5g20480	<i>EFR</i>	385	EF-TU RECEPTOR	1.9	9.0	1.4	1.9	1.8*	0.2	+
At3g11820	<i>SYR121</i>	387	SYNTAXIN OF PLANTS 121	26.5	94.4	19.4	21.3	1.8**	0.1	+
At4g33300	<i>ADR1-L1</i>	399	ADR1-LIKE 1	41.4	142.9	35.5	32.8	1.8**	-0.1	+
At5g45110	<i>NPR3</i>	405	NPR1-LIKE PROTEIN 3	9.7	34.9	6.7	7.6	1.7**	0.2	+
At3g20600	<i>NDR1</i>	414	NON RACE-SPECIFIC DISEASE RESISTANCE 1	5.9	21.7	3.9	4.9	1.7**	0.2	+
At5g46520	<i>VICTR</i>	418	VARIATION IN COMPOUND TRIGGERED ROOT GROWTH RESPONSE	4.6	17.4	3.7	4.3	1.7**	0.2	+
At5g14930	<i>SAG101</i>	426	SENESCENCE-ASSOCIATED GENE 101	7.8	27.4	7.3	8.5	1.7**	0.2	+
At4g23570	<i>SGT1A</i>	444	interacts with REQUIRED FOR MLA12 RESISTANCE 1 (RAR1)	43.4	138.3	41.1	39.9	1.7**	0.0	+
At5g04720	<i>ADR1-L2</i>	447	ADR1-LIKE 2	22.7	73.1	21.1	22.3	1.6**	0.1	+
At4g16860	<i>RPP4</i>	450	RECOGNITION OF PERONOSPORA PARASITICA 4	41.8	131.2	36.9	44.4	1.6**	0.3	+
At4g19660	<i>NPR4</i>	465	NPR1-LIKE PROTEIN 4	9.9	32.0	4.8	6.8	1.6**	0.4	+
At3g45640	<i>MPK3</i>	470	MITOGEN-ACTIVATED PROTEIN KINASE 3	79.5	240.6	61.2	65.7	1.6**	0.1	+
At1g11310	<i>MLO2</i>	535	MILDEW RESISTANCE LOCUS O2	55.6	145.1	48.3	52.7	1.4**	0.1	+
At5g05190	<i>EDR4</i>	541	ENHANCED DISEASE RESISTANCE4	6.5	18.2	6.8	6.0	1.3*	-0.2	+
At1g64280	<i>NPR1</i>	550	NONEXPRESSER OF PR GENES 1	21.3	54.5	18.0	19.1	1.3**	0.1	+
B At3g22231	<i>PCC1</i>	53	PATHOGEN AND CIRCADIAN CONTROLLED 1	97.6	1066.3	5.3	32.4	3.4**	2.4**	+
At3g22235		121	closest homolog to PCC1	106.4	758.3	11.5	36.3	2.8**	1.6**	+

Figure S2. Pip⁺ Genes Include a Battery of Immune-Regulatory and Defense-Related Genes, Related to Figure 1 and Tables S1 and S2

(A) RNA-seq analyses identified 705 Pip⁺ genes out of a total of 28496 genes with significant Pip-induced upregulation in the Col-0 wild-type. RNA samples originate from leaves of Pip (P) and H₂O (H)-treated plants (see Figure 1). 40 Pip⁺ genes with a characterized role in plant defense are depicted. All of them also constitute SAR⁺ genes (right column). The mean expression values of the three replicates per treatment and genotype (Col-0 and *fmo1*) are shown. In addition, mean log₂-transformed P/H-ratios (fold-changes) are depicted, and asterisks indicate significant changes between P- and H-treatments (**: FDR < 0.001; *: FDR < 0.05). The 705 Pip⁺ genes were listed in descending order from higher to lower Col-0 P/H ratios (see Table S1), and the position of the genes in the list is indicated in column 3.

(B) Only two genes were significantly upregulated in *fmo1* in response to Pip-treatment in the RNA-seq covered genome.

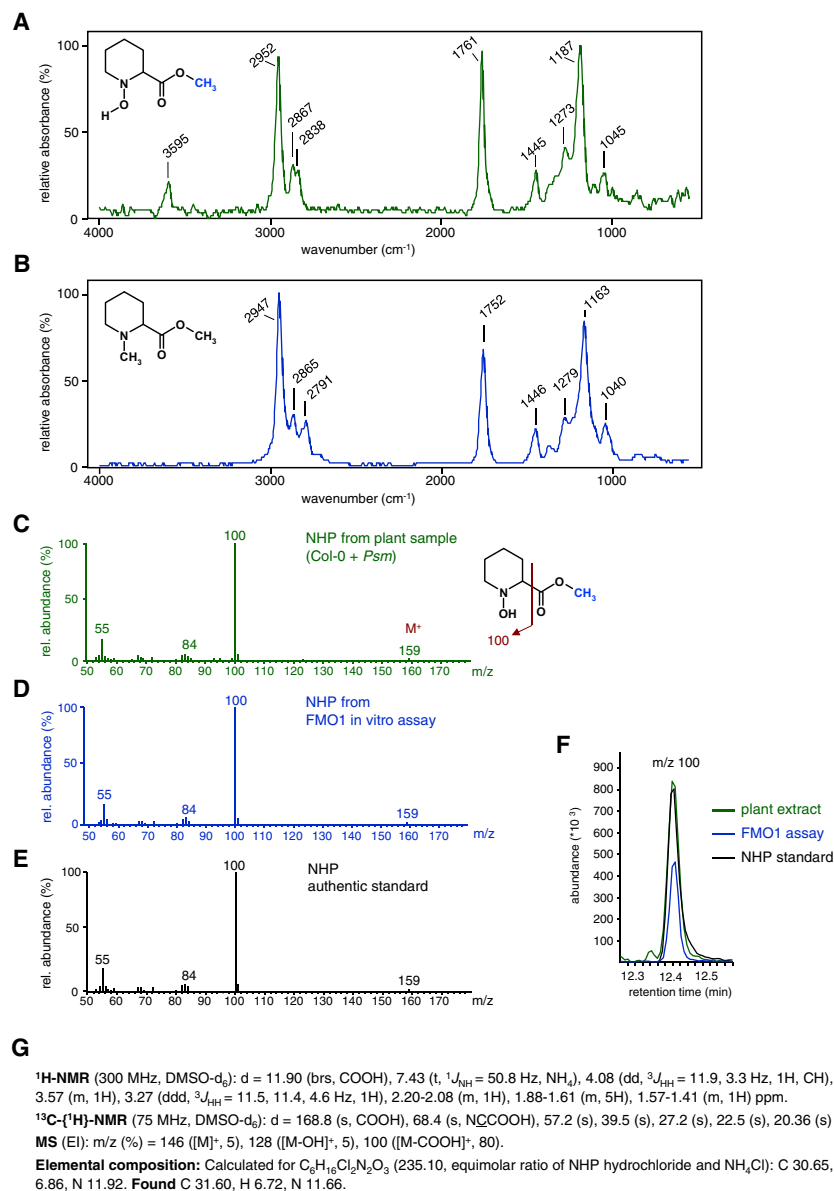


Figure S3. Infrared Spectroscopic and Mass Spectrometric Characterization of N-Hydroxypiperelic Acid, Related to Figure 2

(A) IR spectrum and structure of methylated NHP (**1a**) from plant extracts, as obtained by GC-FTIR analysis (compare Figure 2D). The methyl group (blue) indicated in the molecular formula is introduced by derivatization with trimethylsilyl diazomethane. Assignments of main IR bands to functional group vibrations (wavenumber / vibration): 3595 cm⁻¹ / O-H stretching; 2952 cm⁻¹ / C-H (methyl) stretching; 2867 and 2838 cm⁻¹ / C-H (methylene) stretching; 1761 cm⁻¹ / C=O stretching; 1187 cm⁻¹ / C-O stretching.

(B) IR spectrum and structure of the initially closest hit in the IR database, N-methyl-pipecolic acid methylester.

(A and B) The presence of the O-H stretching vibration (3595 cm⁻¹) in the IR spectrum of methylated NHP (A) and its absence in the IR spectrum of N-methyl-pipecolic acid methylester (B) is the most distinguishing feature of both spectra. Further, the presence of two methyl groups in N-methyl-pipecolic acid methylester causes a more dominant C-H stretching vibration at ~2950 cm⁻¹ in its IR spectrum (B) compared to the IR spectrum of methylated NHP (A) that carries one methyl group only.

(C-F) NHP identified in plant extracts is identical with NHP from *in vitro* FMO1 enzyme assays and with chemically synthesized, authentic NHP.

Mass spectra of methylated NHP (compound **1a**) derived from plant extracts (compare Figure 1A) (C), from biochemical assays with recombinant FMO1 protein and L-Pip as a substrate (compare Figure 1B) (D), and from chemical synthesis (E). The methyl group (blue) indicated in the molecular formula is introduced by derivatization with trimethylsilyl diazomethane. The molecular ion (M⁺) and the fragmentation leading to the main fragment ion of m/z 100 are indicated. (F) Overlay of ion chromatograms (m/z 100) of different GC-MS analyses indicating that methylated NHP from plant extracts (green), FMO1 *in vitro* assays (blue), and chemical synthesis (black) have identical retention times.

(G) Characterization of chemically synthesized NHP (1-hydroxypiperidine-2-carboxylic acid hydrochloride with nearly equimolar amounts of ammonium chloride; see Method Details in the STAR Methods) by ¹H-NMR, ¹³C-NMR, mass spectrometry and elemental analysis.

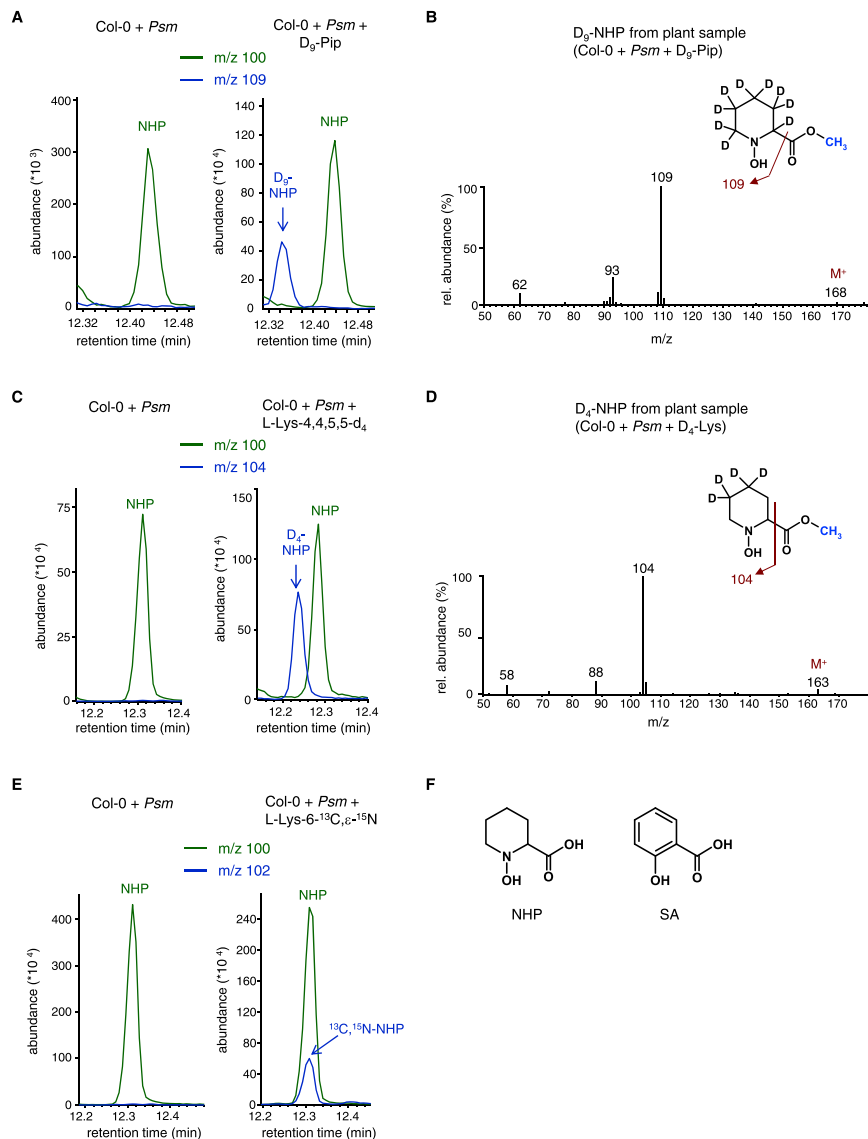


Figure S4. NHP Is Biosynthetically Derived from Pip in Plants and Involves α -Transamination of L-Lys, Related to Figure 2

(A) Feeding of isotope-labeled D_9 -Pip to *Psm*-inoculated Col-0 plants results, in addition to natural NHP (m/z 100), in the formation of D_9 -labeled NHP (m/z 109). Left: overlaid ion chromatograms (m/z 100 and 109) of GC-MS analyzed extract samples from *Psm*-inoculated Col-0 leaves indicate NHP formation. Right: Feeding of D_9 -labeled Pip to *Psm*-inoculated Col-0 causes the additional formation of D_9 -NHP in leaves. GC-MS analysis was performed after analyte methylation with trimethylsilyl diazomethane.

(B) Mass spectrum with indicated M^+ ions and plausible fragmentation patterns of methylated D_9 -NHP, as obtained from the substance peak shown in (A). Please note the shifts in the fragmentation pattern by nine mass units compared to unlabelled **1a** (Figures 2C and S3C). The methyl group introduced by sample derivatization is indicated in blue.

(C) Feeding of isotope-labeled D_4 -Lys to *Psm*-inoculated Col-0 plants results, in addition to natural NHP (m/z 100), in the formation of D_4 -labeled Pip (Hartmann et al., 2017) and D_4 -labeled NHP (m/z 104). Left: overlaid ion chromatograms (m/z 100 and 104) of GC-MS analyzed extract samples from *Psm*-inoculated Col-0 leaves indicate NHP formation. Right: Feeding of D_4 -Lys to *Psm*-inoculated Col-0 causes the additional formation of D_4 -NHP in leaves. GC-MS analysis was performed after analyte methylation with trimethylsilyl diazomethane.

(D) Mass spectrum with indicated M^+ ions and plausible fragmentation patterns of methylated D_4 -NHP, as obtained from the substance peak shown in (C). Please note the shifts in the fragmentation pattern by four mass units compared to unlabelled **1a** (Figures 2C and S3C). The methyl group introduced by sample derivatization is indicated in blue.

(E) Feeding of isotope-labeled L-Lys-6- ^{13}C , ϵ - ^{15}N to *Psm*-inoculated Col-0 plants results, in addition to natural NHP (m/z 100), in the formation of ^{13}C , ^{15}N -labeled NHP (m/z 102). The ϵ -amino group of L-Lys is therefore found in both Pip (Hartmann et al., 2017) and NHP within the *Arabidopsis* biosynthetic pathway. Further details as described in (C).

(F) Molecular structures of N-hydroxypipicolinic acid (NHP) (left) and salicylic acid (SA) (right).

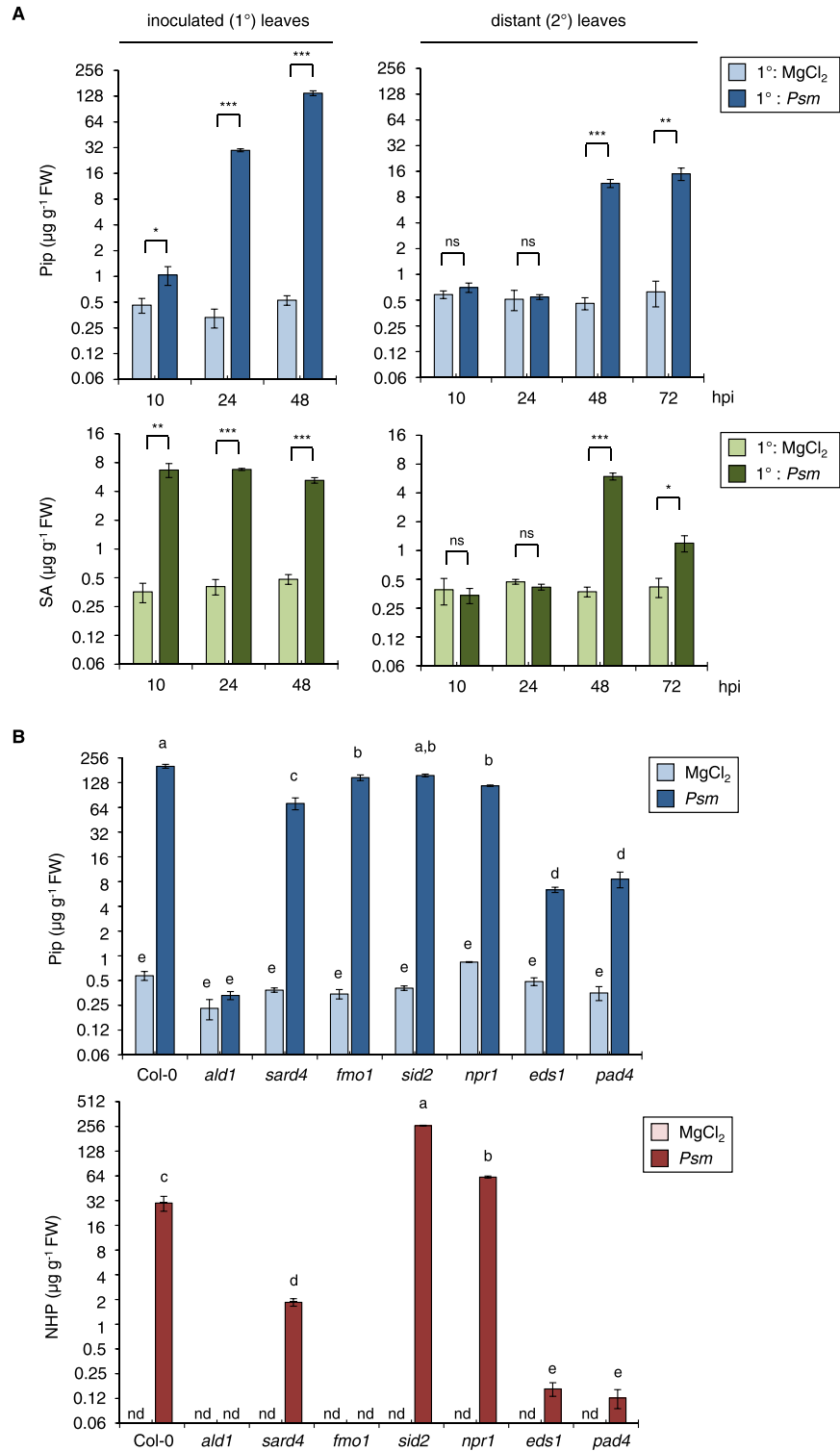


Figure S5. N-Hydroxypipelic Acid, Pipelic Acid, and Salicylic Acid Accumulation in Leaves of Arabidopsis Plants following *P. syringae* *pv. maculicola* Inoculation, Related to Figure 3

(A) Time course of pipelic acid (Pip) and salicylic acid (SA) accumulation in inoculated (1°) and distant (2°) leaves of *Arabidopsis* Col-0 following *P. syringae* *pv. maculicola* (*Psm*) inoculation (Related to Figure 3A). Levels of Pip (blue) and SA (green) [$\mu\text{g g}^{-1}$ leaf fresh weight (FW); hpi: hours post inoculation]. Inoculation details as described in Figure 3A. Data represent the mean \pm SD of at least three biological replicates. Asterisks denote statistically significant differences

(legend continued on next page)

between *Psm*- and mock (MgCl_2)-treated samples of a given point of time (* $p < 0.05$; ** $p < 0.01$; *** $p < 0.001$; two-tailed t test). Please note that the y-axes are presented in logarithmic (\log_2) scaling.

(B) Pip and N-hydroxypipicolic acid (NHP) levels in different *Arabidopsis* lines at 48 h post inoculation (Related to [Figures 3B and 3C](#)). Levels of Pip (blue) and NHP (red) in *Psm*-inoculated and 10 mM MgCl_2 -infiltrated (mock-control) leaves of Col-0 and different mutant plants at 48 hpi. Data represent the mean \pm SD of at least three biological replicates. Different letters above the bars denote statistically significant differences ($p < 0.05$, ANOVA and post hoc Tukey HSD test). The y-axes have logarithmic (\log_2) scaling.

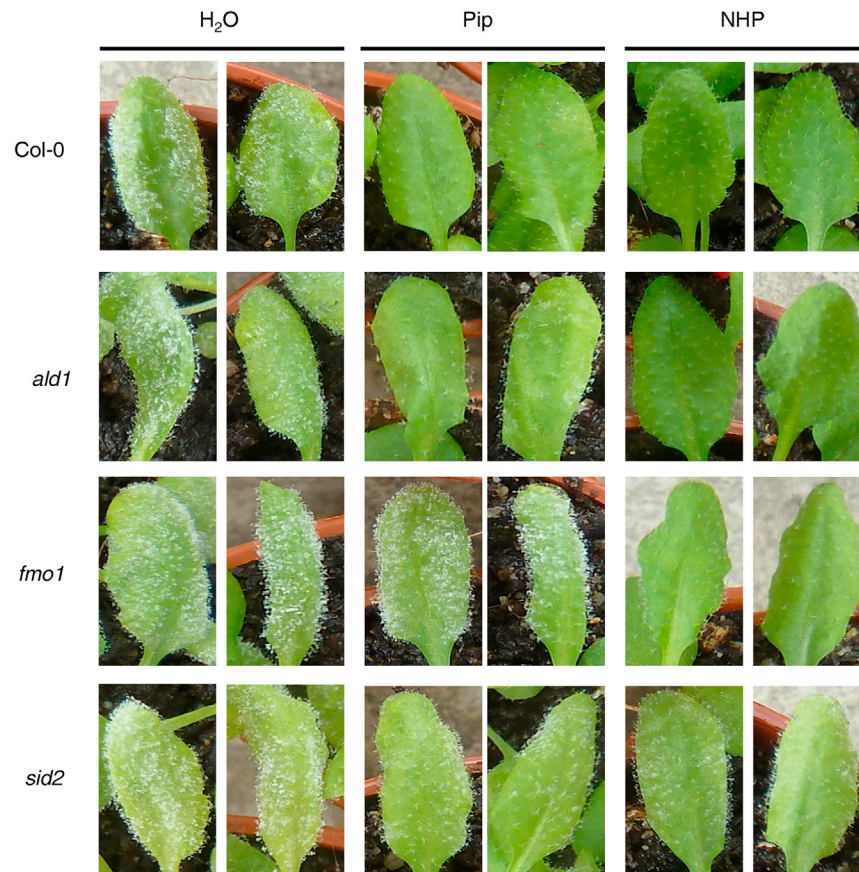


Figure S6. Exogenous NHP Effectively Protects *Arabidopsis* from Invasion by the Oomycete *Hyaloperonospora arabidopsidis* and Mediates, in Contrast to Pip, Acquired Resistance to *fmo1*, Related to Figures 6 and 7

2 week-old *Arabidopsis* Col-0, *ald1*, *fmo1*, and *sid2* plants were pretreated with Pip (middle) or NHP (right) as described in Figure 5A. Non-pretreated control plants (left) and pretreated plants were spray-inoculated with a suspension of 5×10^4 ml^{-1} sporangia of the compatible *Hpa* isolate Noco2. Plants were photographed 7 days after inoculation to visualize their symptomology. 2 representative leaves for each case are depicted. Please refer to Figure 6 for further information.

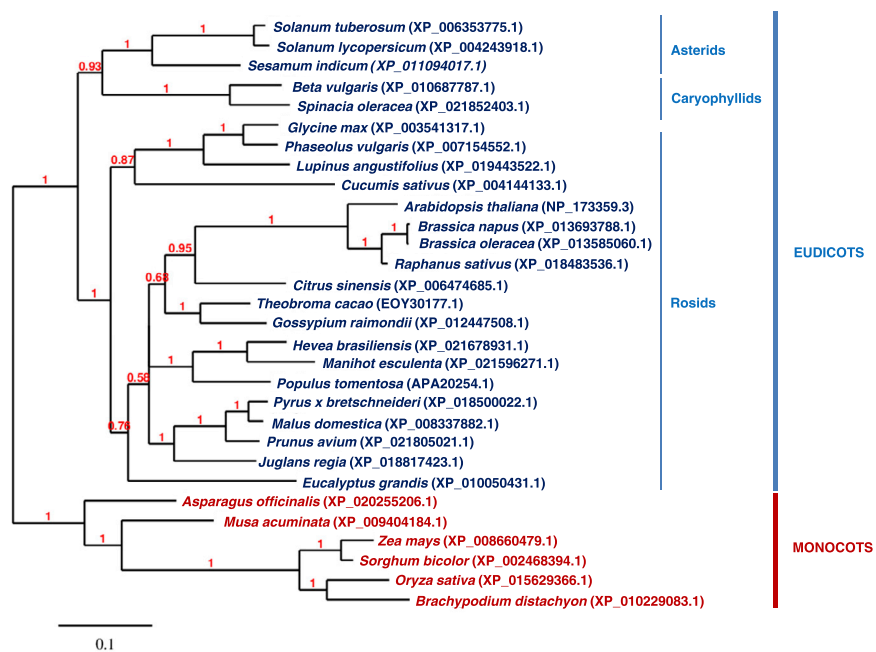


Figure S7. Phylogenetic Analysis of Potential FMO1 Orthologs from Selected Monocots and Dicots, Related to STAR Methods

The AtFMO1 protein sequence (NP_173359.3) was used in a Blast search (<https://blast.ncbi.nlm.nih.gov/Blast.cgi?PAGE=Proteins>) against protein databases of other plant species (Monocotyledoneae - taxid:4447 and eudicots - taxid:71240). The phylogenetic analysis was performed using the Phylogeny.fr analysis pipeline (<http://www.phylogeny.fr/phylogeny.cgi>) and visualized as “non-rooted” phylogenetic tree, built based on Bayesian inference (Dereeper et al., 2008). The confidence values are shown on the branches and the scale bar represents the number of amino acid changes per site.